A Novel Fractional-Order Variational Approach for Image Restoration Based on Fuzzy Membership Degrees

MUSHTAQ AHMAD KHAN[1], **ASMAT ULLAH**[2], **SAHIB KHAN**[3], **MURTAZA ALI**[1], **SHERAZ KHAN**[1], **KHALIL KHAN**[4], **MEHEDI MASUD**[5], (Senior Member, IEEE), AND **JEHAD ALI**[6,7]

[1]Department of Electrical Engineering, University of Engineering and Technology Mardan, Khyber Pakhtunkhwa 23200, Pakistan
[2]Department of Education, University of Engineering and Technology Peshawar, Peshawar 74800, Pakistan
[3]Department of Electrical Electronics and Communications Engineering, 10129 Politecnico di Torino, Italy
[4]Department of Information Technology and Computer Science, Pak-Austria Fachhochschule: Institute of Applied Sciences and Technology, Haripur 22620, Pakistan
[5]Department of Computer Science, College of Computers and Information Technology, Taif University, Taif 21944, Saudi Arabia
[6]Department of Computer Engineering, Ajou University, Suwon 16499, South Korea
[7]Department of AI Convergence Network, Ajou University, Suwon 16499, South Korea

Corresponding author: Mehedi Masud (mmasud@tu.edu.sa)

ABSTRACT We propose a new fractional-order (space and time) total variation regularized model for multiplicative noise removal in this research article. We use the regularly varying fuzzy membership degrees to characterize the likelihood of a pixel related to edges, texture regions, and flat regions to improve model efficiency. This approach is capable of maintaining edges, textures, and other image information while significantly reducing the blocky effect. We opt for the option of local actions. In order to efficiently find the minimizer of the prescribed energy function, the semi-implicit gradient descent approach is used (which derives the corresponding fractional-order Euler-Lagrange equations). The existence and uniqueness of a solution to the suggested variational model are proved. Experimental results show the efficiency of the suggested model in visual enhancement, preserving details and reducing the blocky effect while extracting noise as well as an increase in the PSNR (dB), SSIM, relative error, and less CPU time(s) comparing to other schemes.

INDEX TERMS Fractional-order total variation, time and space fractional derivative, Grünwald-Letniko derivative, Caputo derivative, multiplicative noise, fuzzy membership degrees.

I. INTRODUCTION

I mage restoration is an inverse problem that has been extensively explored in the fields of image processing and computer vision. A real captured image may be degraded by some unavoidable random elements. These undesirable factors are known as noise and can be of various nature. The primary objective of the de-noise is to extract these unexpected elements from the image. In this way, the method of approximating the undiscovered image of interest from the degraded image given is recognized as restoring the image and has many applications in various fields.

The associate editor coordinating the review of this manuscript and approving it for publication was Chih-Yu Hsu.

Applications involving reconstruction operations vary from materials science, astronomy, genetics, chemicals, humanities, geophysics, hydrology, mechanics, remote sensing, and other areas, including imaging methods [1]. In recent years, several methods such as variational, Fourier, wavelet, Laplace, fractional Fourier transforms, singular value decomposition filters, non-local filters, anisotropic diffusion etc. have been applied in various image restoration problems for suppressing noise [2]. Several noise types, such as additive (Gaussian) noise [3], impulse noise [4], Cauchy noise [5], and Poisson noise [6], were investigated in the literature.

Noise is typically modelled as Gaussian noise in various image processing methods: given a true u image and is expected to be distorted by the n additive (Gaussian) noise.

The target is to restore u from $f = u + n$ data. There are numerous successful approaches to handle this issue. Stochastic methods, wavelet methods, principal component analysis-based methods, and variational methods presented in [7] are among the many significant ones. The variational model contains two titles; a data fitting term and a filter (regularizer). It is understandable that variational systems have been taken into consideration by explicitly estimating the reflection of the fundamental scenario and sometimes showing successful outcomes in the image noise removal query. Total variation technique has been commonly used for the image restoration process owing to the edge preservation and image restoration process. The image structure is framed as a function belonging to the bounded variation space (BVS) in (1) the ROF model and hence supports a constant function in the bounded variation space that normally contributes to the staircase effect, (ii) Better image features and information cannot be maintained by the ROF model [8]. The L^2-norm cannot differentiate between various oscillating components with various frequencies, for instance noise and texture, according to [9], and thus the textures are cleaned with noise during the image recovery process. For more details see [10], [11].

Practically speaking, there are other kinds of noise also, for example, multiplicative noise likewise contaminates an image. In this work, we concentrate on the problem of removing multiplicative noise (That is integral to the study of coherent frameworks of imaging and occurs in various practices). Particularly, the restoration of medical, synthetic aperture radar (SAR), synthetic, real-life, and general images [12]. Supposition is if any multiplicative noise η has degraded the actual image u, so the goal is to get u for the information $f = u\eta$ that carries a Gamma law with a mean of 1 and variance is a function of the image magnitude [13]. Its probability density function (PDF) can be expressed as below.

$$G_\eta = \frac{1}{\Gamma(k)} \eta^{k-1} e^{-a}; \{k > 0\}, \tag{1}$$

where a Gamma function is $\Gamma(\bullet)$ and an integer is by k.

Multiplicative noise (also recognized as speckle) is inescapably preceded by images proliferated by coherent imaging frameworks like synthetic aperture radar (SAR), medical, and laser images owing to the coherent nature of dissipating phenomena [14]. The multiplicative noise interferes seriously with higher assignments, for example, target detection or object recognition, image segmentation, image classification, and image enhancement, and so forth. Because of the coherent structure of the image capture process, the noise range is populated by the actual picture in the multiplicative noise models and is portrayed by non-Gaussian probability density functions, withholding the fundamental models of Gamma and Rayleigh [15]. The variance, which is a function of the transmitted signal [16], is non-Gaussian, independent, and temporally dependent. Consequently, the expulsion of multiplicative noise is an exceptionally testing assignment analyzed with Gaussian noise [17]. To the best of our

knowledge, the famous de-speckling approaches include non-local filtering, wavelet-based, spatial and variational [18]. In this study, we will concentrate on the variational approach based on fractional-order for the reconstruction of images contaminated with multiplicative noise. As far as we could remember, there are a few variational approaches concerned about the issue of multiplicative noise removal [19], [20]. For further details, the readers are referred to [21]–[25].

Fractional calculus is a fast developing mathematical subject, which gives a significant tool for non-local field theories and as such fractional-order PDEs based methods established to be a robust tool for image, signal, video, and optical fringe processing [26]. The primary aim behind this development is the aim that the use of fractional calculus in image restoration problems would encourage an increasingly successful and efficient technique to deal with staircase impact and fine-scale features issues. In recent years, the idea of fractional operator and measure has been considered widely in numerous engineering fields such as electrochemistry, control theory, neuronal model, and so on [27]. In image restoration problems, fractional-order derivative-based operators have a great capacity to handle fine-scale characteristics such as edges and textures. They are additionally applied to enhance the quality of images in edge detection, segmentation, restoration, shape analysis, tracking, pattern, face, and action recognition. Furthermore, lengthy memory is a significant feature of fractional order differentiation and is a predominant difference between integer-order and fractional-order differentiation [28].

The traditional strategies for image restoration problems do not appropriately estimate images involving edges. An approach depends on the total variation minimization norm is implemented in [7] to examine this effect. This scheme was able to obtain a desirable settlement between the removal of noise and the preservation of edges. The images come about because of the use of this approach in the presence of noise anyway will in general produce the purported blocky effects on the images as it supports a piecewise constant solution in bounded variation space. The image characteristics in the true image may not be adequately obtained in this way, and inclinations may provide piecewise constant sections. In research papers and books, various techniques have been developed to reduce the blocked outcomes, thus preserving sharp jump discontinuities. The enhanced total variation (TV) schemes are divided into two classes; the high-order derivative and the derivative of the fractional-order. For instance, a fourth-order partial differential equation-based image de-noising model was introduced by [29]. It has been demonstrated that this model can manage the staircase issue. In any case, it activates the indication of uplifting impact and the creation of edge artifacts. An enhanced fourth-order PDE model based on [30], [31] has been developed to deal with this issue.

Several fractional-order derivative-based models were presented in [32]–[34] for Gaussian noise and multiplicative noise removal as a trade-off within the first order
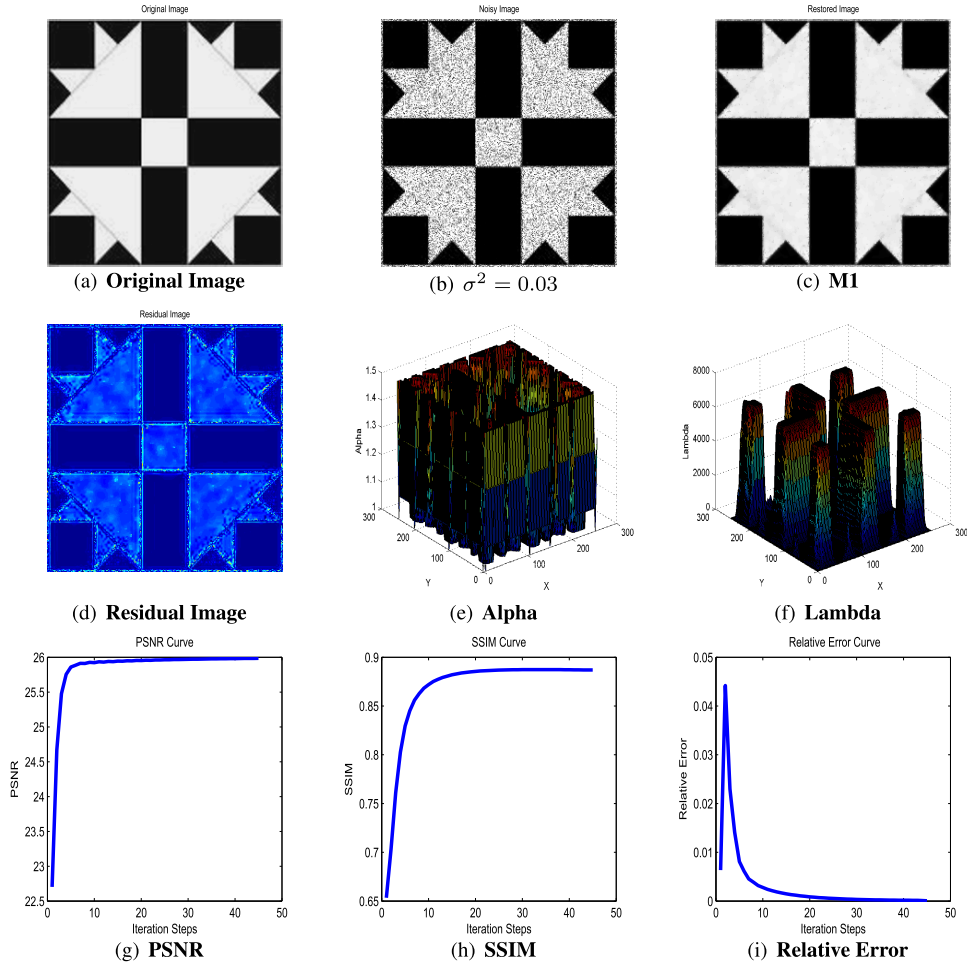
FIGURE 1. a) True image 256^2; b) Degraded image with $\sigma^2 = 0.03$; c) Denoised image; d) Residual image;
e) Adaptive value of α; f) Adaptive value of λ; g) PSNR result; h) SSIM result; i) Relative error result respectively.

TABLE 1. Performance of the proposed model (M1) on synthetic images of size (256^2) and (512^2) contaminated by multiplicative noise of variance $\sigma^2 = 0.03$ and 0.2 in terms of PSNR (db), SSIM, relative error and CPU time (s) results.

Problem	σ^2/L	image size	Proposed Model (M1)			
			PSNR (db)	SSIM	Relative Error	CPU Time (s)
Fig.1	0.03	256^2	25.98	0.8731	0.005	6.94
Fig.2	0.2	512^2	46.34	0.9975	0.000015	31.86

TABLE 2. Performance of the proposed model (M1) on natural images of size (1820 × 720), (256^2) and (512^2) degraded by multiplicative noise of variance $\sigma^2 = 0.02$, 0.2 and 0.3 and $L = 5$, regarding PSNR (db), SSIM, relative error and CPU time (s) results.

Problem	σ^2/L	image size	Proposed Model (M1)			
			PSNR (db)	SSIM	Relative Error	CPU Time (s)
Fig.3	5	1820 × 720	26.73	0.8022	0.000122	56.24
Fig.4	0.02	256^2	31.70	0.9045	0.005	7.34
Fig.5	0.2	256^2	29.55	0.8457	0.005	7.06
Fig.6	0.3	256^2	30.02	0.8857	0.005	6.20

total variation regularized models and high order deriva-
tive based models, and thus used for super-resolution and
image restoration [9]. By correctly choosing the order of
the derivative, they will ease the disagreement between stair-
case effect reduction and edge conservation. In addition,
the fractional-order derivative driver has a "non-local" behav-
ior on the ground that the fractional-order derivative at a
position is centered on the features of the whole function and
not merely the values in the vicinity of the [35] point, which
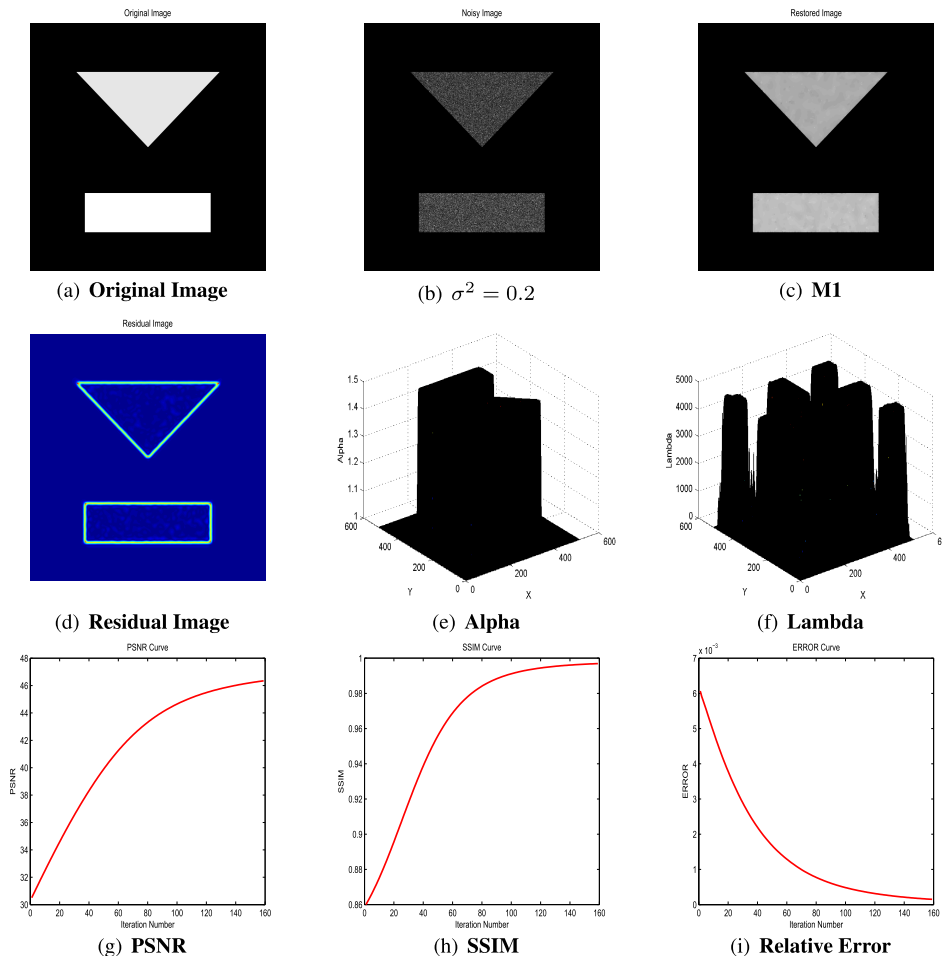is useful for enhancing the presentation of the preservation

FIGURE 2. a) Given image 512^2; b) Noisy image with $\sigma^2 = 0.2$; c) De-noised image; d) Residual image; e) Adaptive value of α; f) Adaptive value of λ; g) PSNR result; h) SSIM result.

of the texture. Experimental findings reveal that writing [38] has demonstrated that the fractional-order derivative operates properly to retain textures and reduce the impact of the staircase effect. Pu *et al.* in [39] addressed the kinetic physical value of the fractional-order derivative and suggested fractional investigation models for image texture data. In [40], it has been shown that the fractional-order derivative operator complies more with the oblique inhibition theory of the biological visual framework than the integer-order derivative.

In this study, we consider a discrete class of fractional-order derivative introduced by Grúwald-Letnikov (G-L). The fractional-order derivative is indicated as function operator ∇^α, that can be stated as under.

$$\nabla_{x_1}^\alpha \Phi(x_1, x_2) = \lim_{\Delta x_1 \to 0^+} \frac{\sum_{k \geq 0}(-1)^k C_\alpha^k \Phi(x_1 - k\Delta x_1, x_2)}{(\Delta x_1)^\alpha}$$

$$\nabla_{x_2}^\alpha \Phi(x_1, x_2) = \lim_{\Delta x_2 \to 0^+} \frac{\sum_{k \geq 0}(-1)^k C_\alpha^k \Phi(x_1, x_2 - k\Delta x_2)}{(\Delta x_2)^\alpha} \quad (2)$$

where $C_\alpha^k = \frac{\Gamma(\alpha+1)}{k!\Gamma(\alpha-k+1)}$ is the binomial generalized coefficient with $\Gamma(\bullet)$ is the Gamma function. Until constructing

the finite difference approximate equation of the proposed model, the following concepts of fractional derivative theory are formulated.

Definition 1: The Riemann-Liouville (R-L) fractional-integral operator J^β is given as

$$J^\beta \Phi(x_1) = \frac{1}{\Gamma(\beta)}\int_0^{x_1}(x_1 - t)^\beta \Phi(t)dt; \ \beta > 0, x_1 > 0 \quad (3)$$

Definition 2: The Caputo's fractional-order partial derivative operator $^C\nabla_a^\beta$ of order β is formulated as

$$^C\nabla_a^\beta \Phi(x_1) = \frac{1}{\Gamma(m-\beta)}\int_0^{x_1}\frac{\Phi^m(x_1)}{(x_1 - t)^{\beta - m + 1}}dx_1; \ \beta > 0 \quad (4)$$

with $m - 1 \leq \beta \leq m, m \in N$, where $x_1 > 0$. Caputo's fractional partial derivative of order β being employed to discretize the time-fractional diffusion equations. This time-fractional order derivatives are used to preserve edges in highly oscillatory regions [38].

The goal of this paper is to propose a new fractional-order (space and time) total variation regularized model for removing multiplicative noise and a fast methodology for achieving a numerical solution. In order to develop the proposed
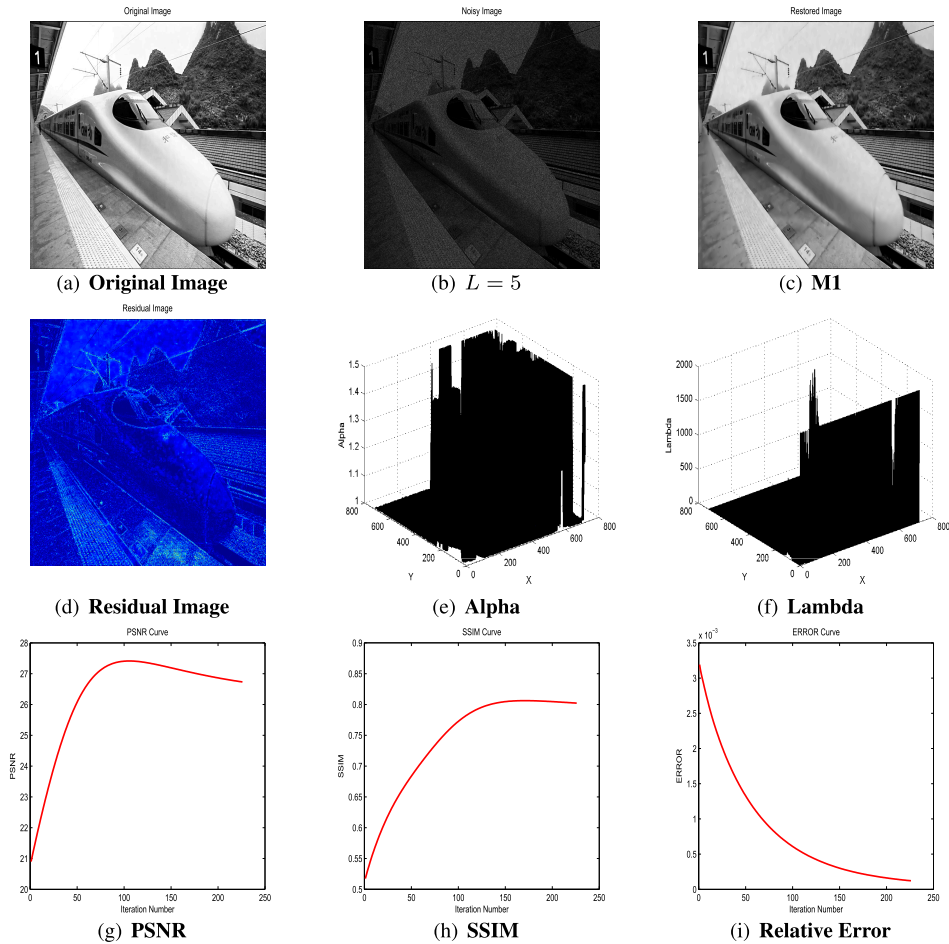
FIGURE 3. a) Original image 1820 × 720; b) Noisy image with $L = 5$; c) De-noised image; d) Residual image; e) Adaptive value of α; f) Adaptive value of λ; g) PSNR result; h) SSIM result; i) Relative error result respectively.

model efficiency, the fractional-order total variation based regularizer is coupled with the inconstant fuzzy membership degrees (FMDs) to increase the probability of a pixel connected to edges, textures and flat regions contributing to better restoration results. The combined strategy works well to preserve image information while substantially reducing the effect of the staircase through the noise removal process. For more reliable restoration results, we take the values of the parameters adaptively and presented their automatic tuned values in figures given below. The existence and uniqueness of a solution to the recommended model are also provided. We communicate simulation findings which show that the suggested model has created a remarkable development in the quality of the restored pictures, both qualitatively and quantitatively.

The entirety of the article is structured as follows. Section 2 examines in detail the three fuzzy membership degrees used in the planned work to boost the outcomes of the reconstruction. In section 3, our newest fractional-order, total variational model to answer the question is presented and illustrates its existence and uniqueness. For the solution of non-linear Euler Lagrange fractional-order PDEs,

a semi-implicit gradient descent scheme is used in section 4. Some reconstruction results of natural and synthetic images are provided in section 5 to display the efficiency of the proposed model. Finally, in section 6, we end with some closing remarks and recommendations for future studies.

II. FUZZY MEMBERSHIP DEGREES (FMDs)

Focused on [35], we adopt the given three FMDs for each (i, j) pixel to express the likelihood of a pixel combined to sides, textured, and smooth areas.

1) THE FMD MATRIX OF EDGES

The primer recovered image u_r mostly consists of edges and flat regions. The edges can be detected by utilizing the edge pointers, for example, the Canny edge detector. In any case, because of the blocky effect brought about by the total variation filter, the observed edges frequently consist of pseudo edges. The Gaussian filter is utilized to distribute suggested pseudo edges before the Canny edge locator. The binary suggestive function of the edges can be described as

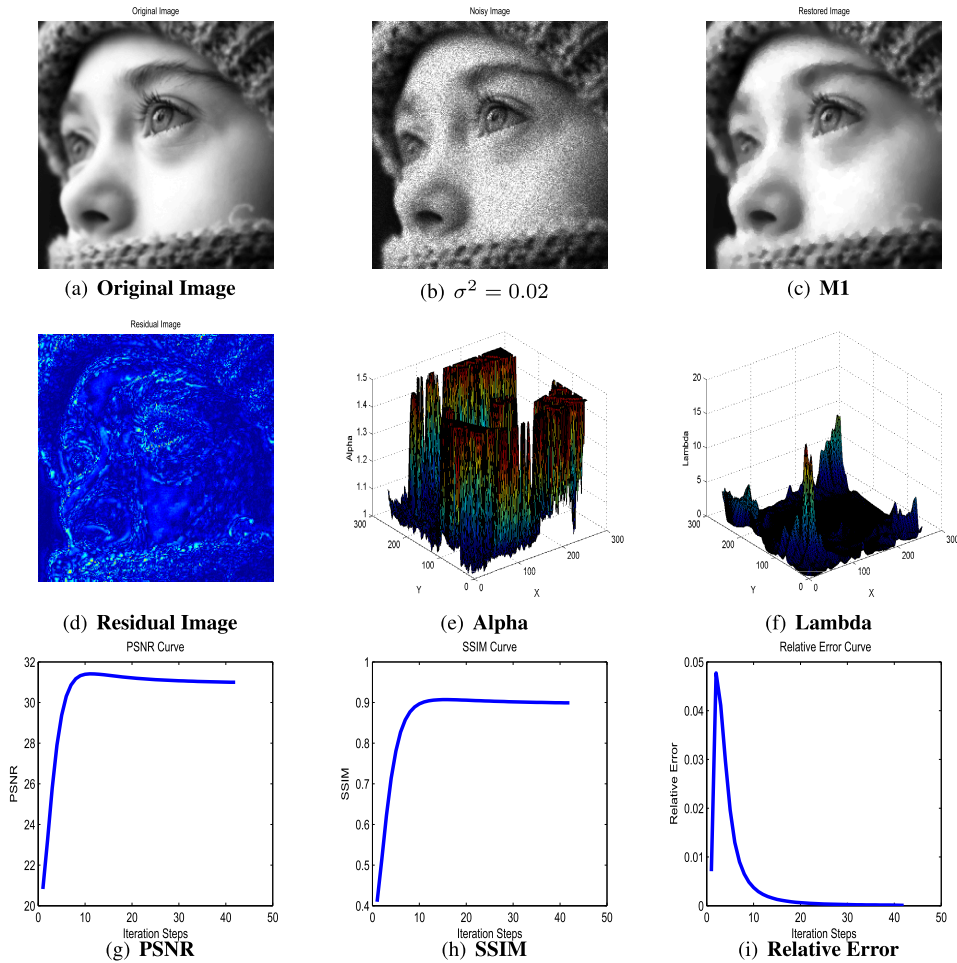$$\Upsilon_E = \Lambda(\chi_1 * u_r) \tag{5}$$

(a) **Original Image**

(b) $\sigma^2 = 0.02$

(c) **M1**

(d) **Residual Image**

(e) **Alpha**

(f) **Lambda**

(g) **PSNR**

(h) **SSIM**

(i) **Relative Error**

FIGURE 4. a) True image 256^2; b) Noisy image with $\sigma^2 = 0.02$; c) De-noised image; d) Residual image; e) Adaptive value of α; f) Adaptive value of λ; g) PSNR result; h) SSIM result; i) Relative error result respectively.

where $\Lambda(\bullet)$ indicates a Canny edge detector, $\chi 1$ is a 2-D Gaussian window, and $*$ is a convolution.

In any circumstance, the pointed edges are usually not accurate in reality. In practice, the pixels around the point edges are compared to the real edges. To handle this, we represent the FMD to characterize the occurrence of each pixel of the image relates to edges. The FMD matrix (Ξ) of edges marked as $\Xi_E = [\Xi_E(i,j)]_{i,j=1}^N$ can be formulated by

$$E_B = \chi_2 * \Upsilon_E,$$
$$\Xi_E(i,j) = \frac{E_B(i,j)}{\max_{i,j=1,2,...,N}\{E_B(i,j)\}} \quad (6)$$

where χ_2 denotes 2-D Gaussian window of size 5^2. Recently, some new schemes have been utilized for edge detection for instance, multiscale gradient edge detection and hybrid edge detection method and hence some good results have been obtained. For further details, see [36], [37].

2) THE FMD MATRIX OF TEXTURED REGIONS

In this research article, the threshold is first discussed and a tentative indicative feature ΥT^{pre} of the textured regions is

adaptively obtained iteratively as in [35]. Anyhow, the regions showed by Υ_T^{pre} have isolated points or fragments which cannot be ordered into textured regions. The modified binary suggestive function of the textured areas has therefore been formulated as

$$\Upsilon_T(i,j) = 1, (\chi_1 * \Upsilon_T^{pre})_{i,j} \geq 0.5,$$
$$= 0, \text{ otherwise },\quad (7)$$

where χ_1 represents 2-D Gaussian window. Likewise, in the case of edges, pixels close to the textured areas detected to relate to the actual textured areas which often include edges. To differentiate between these two distinct items, we describe the FMD matrix of textured regions denoted as (Ξ_T) can be defined as

$$T_{Blur} = (1 - \Xi_E).(\chi_2 * \Upsilon_T),$$
$$\Xi_T(i,j) = T_{Blur}(i,j) / \max_{i,j=1,2,...,N}\{T_{Blur}(i,j)\},\quad (8)$$

where χ_2 indicates the 2-D Gaussian window of size 5×5.

(a) **Original Image**   (b) $\sigma^2 = 0.2$ (c) **M1**

(d) **Residual Image**   (e) **Alpha**   (f) **Lambda**

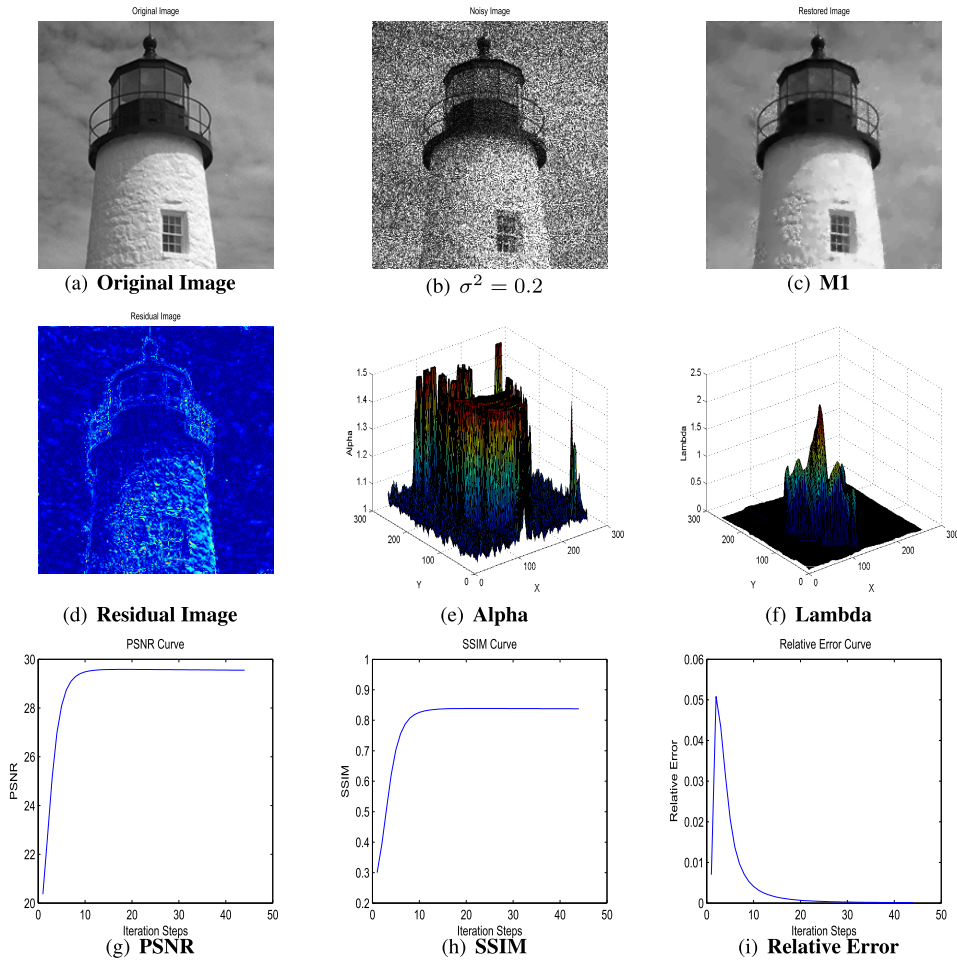(g) **PSNR**   (h) **SSIM**   (i) **Relative Error**

FIGURE 5. a) True image 256^2; b) Degraded image with $\sigma^2 = 0.2$; c) De-noised image; d) Residual image;
e) Adaptive value of α; f) Adaptive value of λ; g) PSNR result; h) SSIM result; i) Relative error result respectively.

3) THE FMD MATRIX OF FLAT REGIONS
We presume three types of regions in this article (edge, texture and flat) and one must be the sum of the probability of each variable relating to them. Therefore, centered on (6) and (8), the FMD matrix ΞF of the flat regions can be expressed in the form

$$\Xi_F(i, j) = 1 - \Xi_E(i, j) - \Xi_T(i, j) \qquad (9)$$

In this section, the FMDs defined the transit step by step at the boundary regions between the edges, the textured and smooth regions, thus reducing the fragment impact caused by the hard threshold.

III. THE PROPOSED IMAGE RESTORATION MODEL (M1)
Motivated by the advantages of fractional order total variation regularizer (FOTVR), a new fractional-order (space and time) total variation regularized model combined with fuzzy membership degrees (FMDs) is recommended for the restoration of images corrupted with multiplicative noise. This model utilizes the benefits of FOTVR and FMDs, contributing to outstanding de-noised outcomes, since in the presence

of newly adopted data fitting term, fractional-order total variation-based regularizer works well to minimize blocky effect, retain sharp edges, low gradient structures, and textures. The model obtained has the advantage of retaining more outstanding picture regions, including edges, textures, and other fine elements, contributing to a more realistic scene while reducing the effect of stairs in smooth areas. Therefore using this model, better changes in PSNR and SSIM values are achieved. The given fractional-order based variational energy functional is proposed to restore a given image degraded with multiplicative noise

$$\hat{u} = \underset{u \in BV^\alpha(\Omega) \cap L^2(\Omega), u>0}{arg \min} \left\{ E(u) = \int_\Omega |\nabla^\alpha u| dx dy + D(f, u) \right\}$$

$$(10)$$

The first term $R^\alpha(u) = \int_\Omega |\nabla^\alpha u| dx dy \approx \sum_{i,j} \{ |\nabla_x^\alpha u_{i,j}| + |\nabla_y^\alpha u_{i,j}| \}$ is the regularizer (filter) and $BV^\alpha(\Omega) = \{ u \in L^1(\Omega) : R^\alpha(u) < +\infty \}$ is the fractional-order bounded variation space of functions. The second term $D(f, u)$ is the data fitting term that evaluates the distortion of the connection
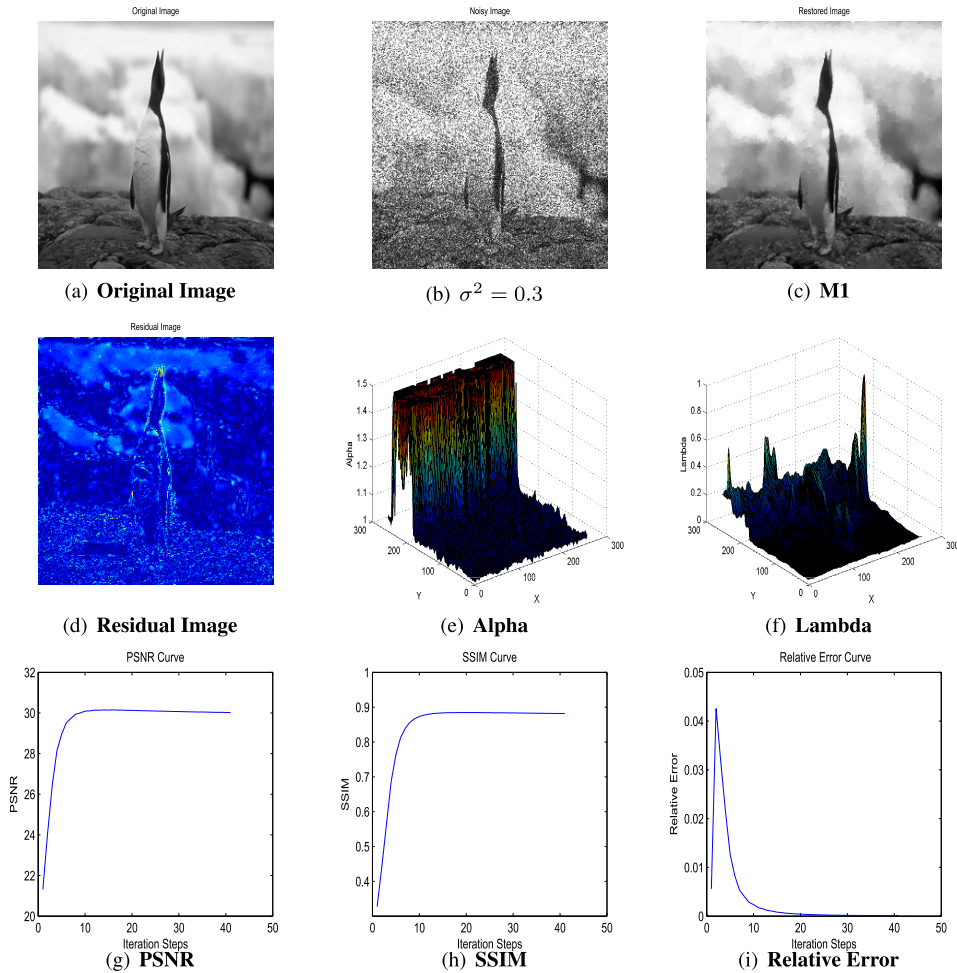
(a) **Original Image** (b) $\sigma^2 = 0.3$ (c) **M1**

(d) **Residual Image** (e) **Alpha** (f) **Lambda**

(g) **PSNR** (h) **SSIM** (i) **Relative Error**

FIGURE 6. a) True image 256^2; b) Degraded image with $\sigma^2 = 0.3$; c) Denoised image; d) Residual image; e) Adaptive value of α; f) Adaptive value of λ; g) PSNR result; h) SSIM result; i) Relative error result respectively.

TABLE 3. Performance of the proposed model (M1) on medical images of size (256^2) and corrupted by multiplicative noise of variance $\sigma^2 = 0.08$, and 0.1 and $L = 5$ regarding PSNR (db), SSIM, relative error and CPU time (s) results.

Problem	σ^2/L	image size	Proposed Model (M1)			
			PSNR (db)	SSIM	Relative Error	CPU Time (s)
Fig.7	0.08	256^2	29.68	0.9048	0.005	8.94
Fig.8	0.1	256^2	30.97	0.9525	0.005	7.68
Fig.9	5	256^2	33.29	0.9458	0.00060	122.88

between u and the observation f and is derived from the MAP. We assume the noise model, based on the work in [25] and is modeled as follow.

$$f = u + \sqrt{u}\eta \qquad (11)$$

where f is the image captured, u is the actual image, η is the multiplicative noise distributed under Rayleigh. Using the logarithmic transform $z = \log u \iff u = e^z$ we can use the subsequent data fitting term along similar lines to Ref. [25] as

$$D(f, u) = \int_\Omega \left(\frac{f}{2} \left(f^2 e^{-z} + z - 2f + e^z \right) + z \right) dxdy \qquad (12)$$

Use the data fidelity term in (12) and then using the exponential transformation $u \to e^u$ for the data fidelity term (12). The energy function (10) can then be reformulated as below.

$$\hat{u} = \underset{u \in BV^\alpha(\Omega) \cap L^2(\Omega), u > 0}{arg\min} \left\{ E(u) \right.$$

$$= \int_\Omega |\nabla^\alpha u| dxdy$$

$$+ \lambda \int_\Omega \left(\frac{f}{2} \left(f^2 e^{-u} + u - 2f + e^u \right) + u \right) dxdy \right\} \qquad (13)$$

where, $BV^\alpha(\Omega)$ is the fractional-order bounded variance function space. The first term is the term for regularization that decides the quality of the u image. $\lambda > 0$ is a parameter
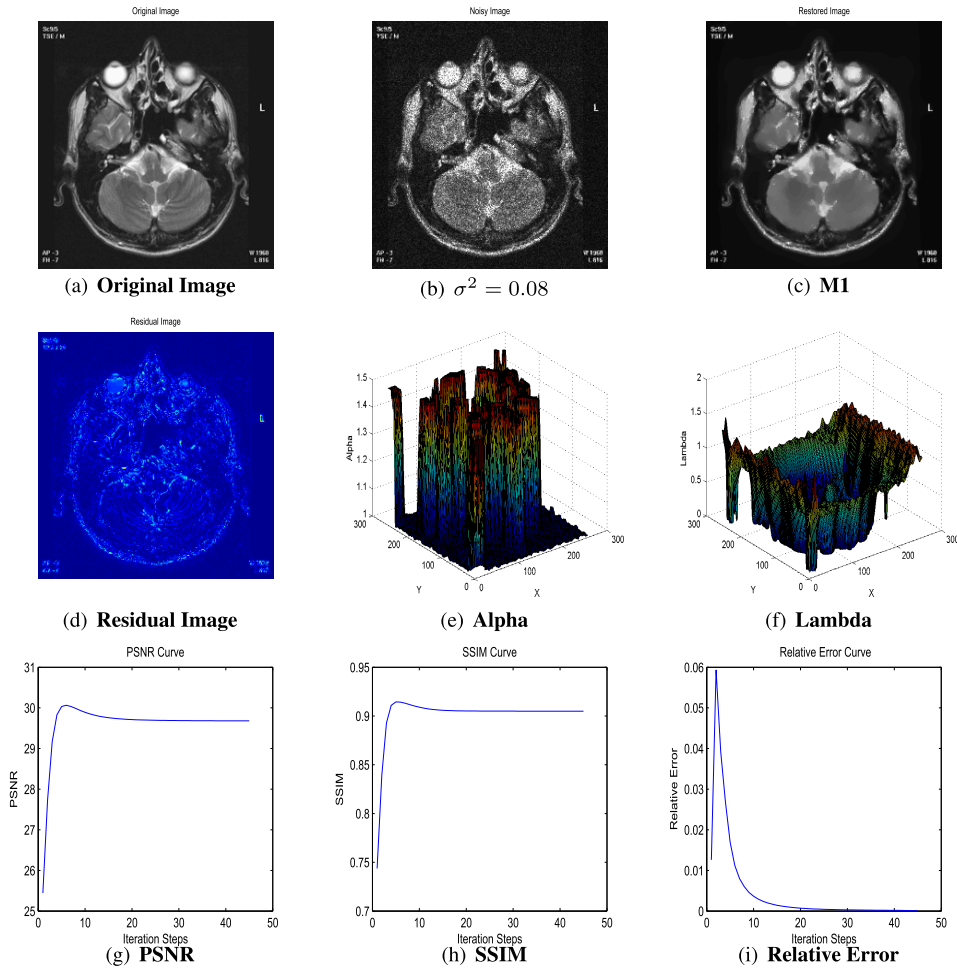
(a) **Original Image** (b) $\sigma^2 = 0.08$ (c) **M1**

(d) **Residual Image** (e) **Alpha** (f) **Lambda**

(g) **PSNR** (h) **SSIM** (i) **Relative Error**

FIGURE 7. a) True image 256^2; b) Degrade image with $\sigma^2 = 0.08$; c) De-noised image; d) Residual image; e) Adaptive value of α; f) Adaptive value of λ; g) PSNR result; h) SSIM result; i) Relative error result respectively.

of regularization. By calculus of variation, the minimization of (13) resulted in the following non-linear Euler Lagrange equation

$$(-1)^\alpha \nabla^\alpha \cdot \left(\frac{\nabla^\alpha u}{\sqrt{|\nabla^\alpha u|^2 + \varepsilon}} \right)$$
$$+\lambda \left(\frac{f}{2}(1 + e^u - f^2 e^{-u}) + 1 \right) = 0 \text{ in } \Omega, \frac{\partial u}{\partial \overrightarrow{n}} = 0 \text{ on } \partial\Omega.$$
(14)

Thus, to prevent singularity, $\varepsilon > 0$ shows the regularized parameter that is chosen near 0. As an evolution parameter, the solution scheme employs a parabolic equation regarding time.

$$\frac{\partial^\beta u}{\partial t^\beta} = (-1)^\alpha \nabla^\alpha \cdot \left(\frac{\nabla^\alpha u}{\sqrt{|\nabla^\alpha u|^2 + \varepsilon}} \right)$$
$$+\lambda \left(\frac{f}{2}(1 + e^u - f^2 e^{-u}) + 1 \right)$$
(15)

where $\beta \in (0, 1)$ is the time fractional derivative. Next, we present a theorem regarding the uniqueness of the proposed model (M1) solution.

Theorem 1: There is a special minimizer in the proposed model (13) at $BV^\alpha(\Omega) \cap L^2(\Omega)$.

This theorem's key aim is to prove the uniqueness of the model suggested. To prove the theorem, we require the following mathematical results.

Lemma 1: The space $BV^\alpha(\Omega)$ is a Banach space.

Lemma 2: (Lower semi-continuity) Let $\{u_k(x)\}$ be a sequence from $BV^\alpha(\Omega)$ which converge in $L^1(\Omega)$ to a function $u(x)$. Then $R^\alpha(u) \leq \lim_{k \to +\infty} \inf R^\alpha(u_k)$.

Lemma 3: The regularizer $R^\alpha(u)$ is convex.

Proof of the previous lemmas can be obtained from lines equivalent to those of Ref. [38].

Proof: The functional function (13) has a special minimizer at $BV^\alpha(\Omega) \cap L^2(\Omega)$, at $BV^\alpha(\Omega) = \{u \in L^1(\Omega) : R^\alpha(u) < +\infty\}$, and is the domain of functional variance bounded by fractional order. According to the optimization theory, the strict convex and coercive properties of an objective functional is responsible for the incomparable minimizer. The $BV^\alpha(\Omega)$ norm is constructed as $\|u\|_{BV^\alpha} = \|u\|_{L^1} + R^\alpha(u)$ whereas $BV^\alpha(\Omega)$, Lemma is a Banach space:Lemma:1 and Lemma:3 is a convex space:$R^\alpha(u)$. the strict convex and
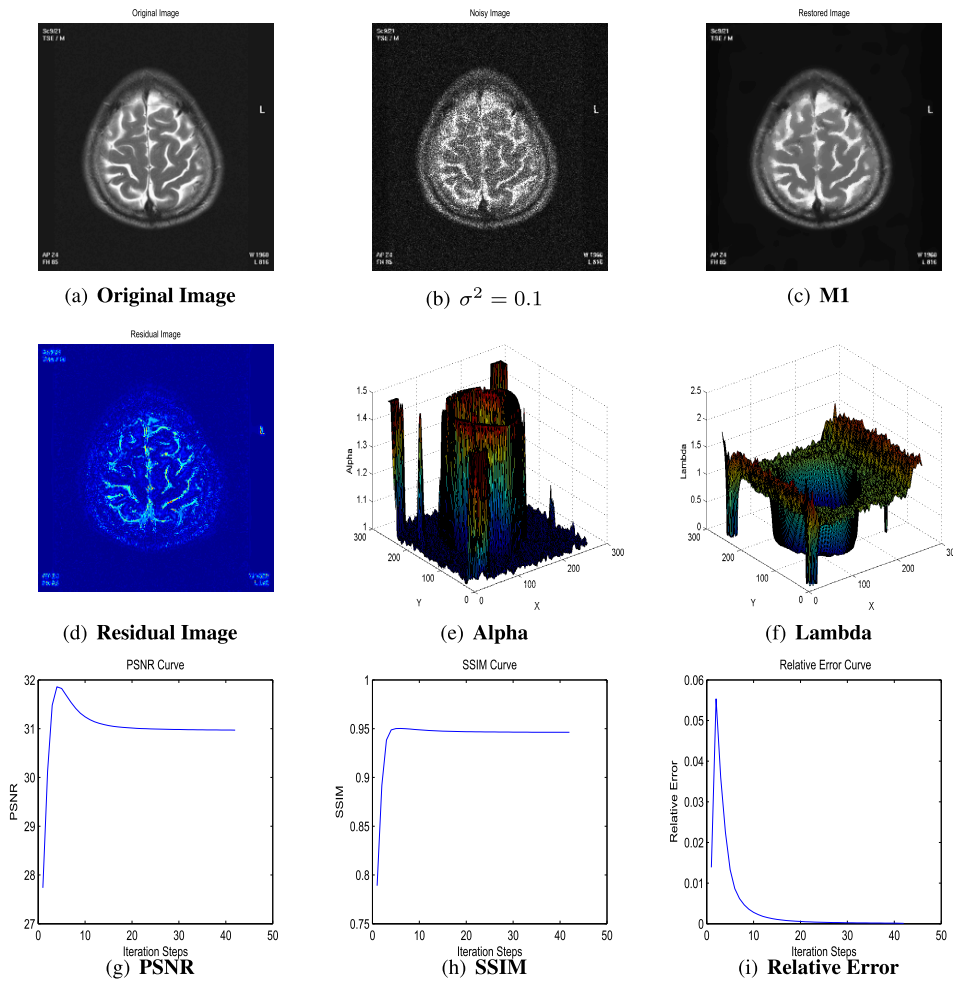
(a) **Original Image** (b) $\sigma^2 = 0.1$ (c) **M1**

(d) **Residual Image** (e) **Alpha** (f) **Lambda**

(g) **PSNR** (h) **SSIM** (i) **Relative Error**

FIGURE 8. a) Given image 256^2; b) Noisy image with $\sigma^2 = 0.1$; c) De-noised image; d) Residual image;
e) Adaptive value of α; f) Adaptive value of λ; g) PSNR result; h) SSIM result; i) Relative error result respectively.

coercive properties of an objective functional is responsible for the incomparable minimizer. The manipulative value of $E(u)$ with $u \in L^1(u)$ matches the value of $E(u) \rightarrow +\infty$ as $\|u\|_{BV^\alpha} \rightarrow +\infty$. We have $D(u, f) \geq 0$ for (13). It means that $\|u\| \leq E(u)$ is up to a constant. The coercive condition, thus, proved to be in $BV^\alpha(\Omega) \cap L^2(\Omega)$ Moreover, the lower semi-continuity is set to $R^\alpha(u)$ by adding Lemma:2. For $D(u, f) \geq 0$, the lower semi consistency still holds. In the end, we conclude that (13) has a lower semi-continuous and coercive solution by typical arguments as E(u). The uniqueness of solution of (13) depends on the formal non- linear Euler-Lagrange equation. Let us denote

$$\dot{D}(u, \lambda) = \lambda \left(\frac{f}{2}(1 + e^u - f^2 e^{-u}) + 1 \right) \quad (16)$$

Describe the appropriate reference energy $E\text{ref}(u)$ for energy $E(u)$ as below.

$$E_{\text{ref}}(u) = \int_\Omega |\nabla^\alpha u| dxdy + \int_\Omega \left(D(u, \lambda) \right) dxdy \quad (17)$$

It is easy to establish that the non-linear Euler-Lagrange equation for $E\text{ref}(u)$ is (14). We have

$$\ddot{D}(u, \lambda) = \lambda \left(\frac{f}{2}(e^u + f^2 e^{-u}) + \frac{f}{2} \left(1 + e^u - f^2 e^{-u} \right) + 1 \right) \quad (18)$$

We consider that $f > 0$ in $L^\infty(\Omega)$ and u is a denoise energy minimizer for $E(u)$, so u is special if $0 < u < f + (f^2 + f)^{0.2}$. We also deduce that $\ddot{D} > 0$ and D are strictly convex. Also $R^\alpha(u)$ is convex by Lemma:3. The functional $E(u)$ is now convex, and $E_{\text{ref}}(u)$ is globally convex and has a special minimizer. This completes the proof.

To solve the non-linear fractional-order (space and time) Euler-Lagrange equation, we introduce the semi-implicit gradient descent scheme in the next section (15).

IV. NUMERICAL IMPLEMENTATION

For the solution of the fractional-order (space and time) non-linear Euler Lagrange equation (15) associated with functional minimization (13), the semi-implicit gradient descent scheme (SIGDS) is implemented in this section. The
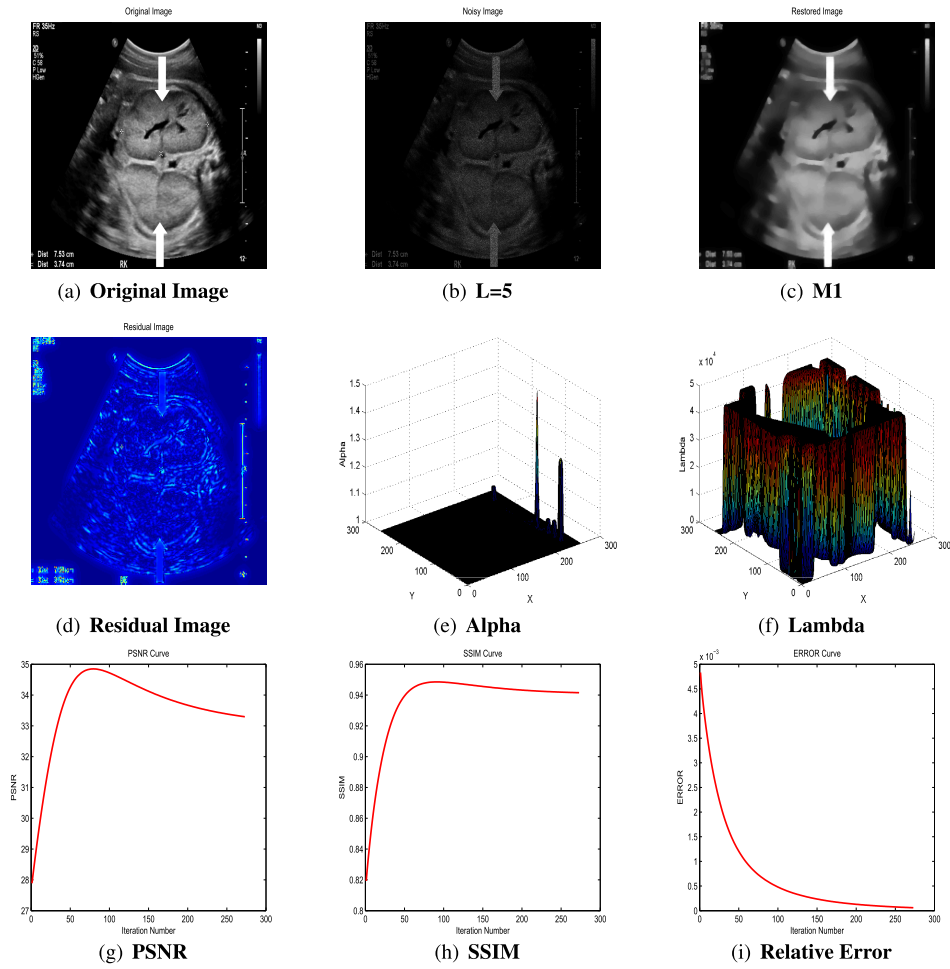
FIGURE 9. a) Given image 256^2; b) Noisy image with $L = 5$; c) De-noised image; d) Residual image; e) Adaptive value of α; f) Adaptive value of λ; g) PSNR result; h) SSIM result; i) Relative error result respectively.

iteration process is not stable if dt is too big and consumes time if it is too small. Assume that the equation (15) is unique and has sufficiently smooth solution under $u(x, y, 0) = u_0$ and the symmetric conditions

$$u_{-1,j}^n = u_{0,j}^n, \quad u_{N+1,j}^n = u_{N,j}^n, \ j = 0, 1, 2, \cdots N;$$
$$u_{i,-1}^n = u_{i,0}^n, \quad u_{i,N+1}^n = u_{i,N}^n, \ i = 0, 1, 2, \cdots N. \quad (19)$$

where $N \times N$ indicates picture dimension. The grid sizes in space and time directions for the finite difference scheme are characterized as $h = \triangle x$, $k = \triangle y$ and $t = \triangle t$, respectively, for all positive entities m and n. To construct the solution domain uniformity grid network, let the grid points in the space interval be defined as $xi = ih, yj = jk$, where $i = 0, 1, 2, ..withm, j = 0, 1, 2, .N$, and the time interval's grid points are represented as $tn = n\triangle t = n\tau, n \geq 1$. For optimal results, we choose $\alpha \in [1, 2]$ and $\beta \in (0, 1)$ adaptively. Moreover, the Grünwald-Letnikov fractional order partial derivatives are used on the variables x and y. The finite

fractional difference can be formulated as

$$\nabla_x^\alpha u_{i,j} = \sum_{k=0}^{K-1} C_k^{(\alpha)} u_{i-k,j}$$
$$\nabla_y^\alpha u_{i,j} = \sum_{k=0}^{K-1} C_k^{(\alpha)} u_{i,j-k} \quad (20)$$

Let $\overline{\nabla}_x^\alpha u_{i,j}$ and $\overline{\nabla}_y^\alpha u_{i,j}$ be the adjoint operators of $\nabla_x^\alpha u_{i,j}$ and $\nabla_y^\alpha u_{i,j}$ and are formulated by

$$\overline{\nabla}_x^\alpha u_{i,j} = \sum_{k=0}^{K-1} C_k^{(\alpha)} u_{i+k,j} \quad \overline{\nabla}_y^\alpha u_{i,j} = \sum_{k=0}^{K-1} C_k^{(\alpha)} u_{i,j+k} \quad (21)$$

where $C^{(\alpha)}k = (-1)^k C^{(\alpha)}k$, the binonmial coefficient is $C^{(\alpha)}k = \frac{\Gamma(\alpha+1)}{\Gamma(k+1)\Gamma(\alpha-k+1)}$, and $\Gamma(\bullet)$ denotes the feature of Gamma. It is also possible to calculate the coefficients of $C^{(\alpha)}k$ from $C^{(\alpha)}0 = 1$, $C^{(\alpha)}k = (1 - \frac{\alpha+1}{k})C^{(\alpha)}k - 1, k = 1, 2, 3 \cdot K - 1$ recursively. The estimated third order computation of the Caputo's fractional partial derivative can be
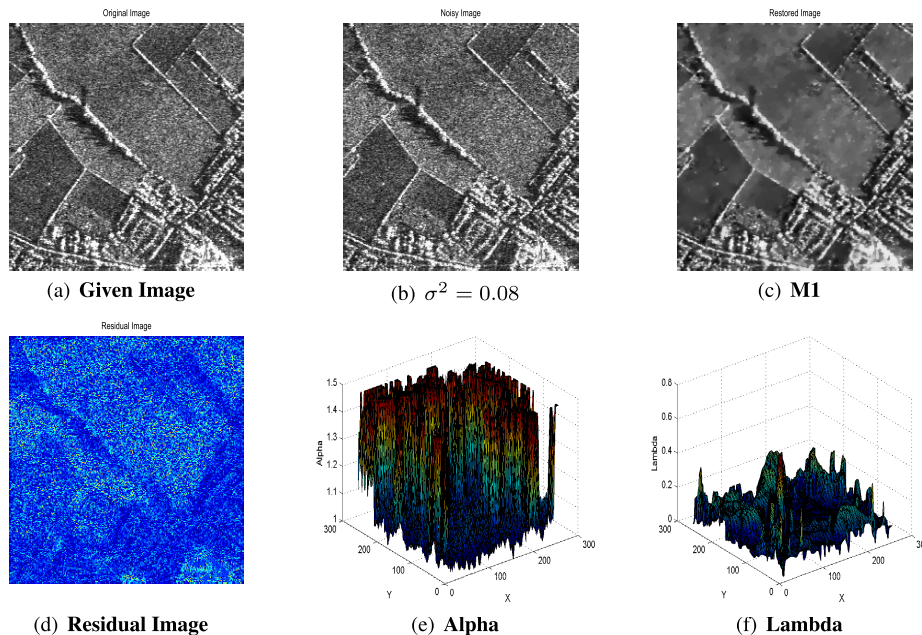
(a) **Given Image**

(b) $\sigma^2 = 0.08$

(c) **M1**

(d) **Residual Image**

(e) **Alpha**

(f) **Lambda**

FIGURE 10. a) Given image 256^2; b) Corrupt image with $\sigma^2 = 0.08$; c) De-noised image; d) Residual image; e) Adaptive value of α; f) Adaptive value of λ respectively.

constructed as

$$D_t^\beta u_{i,j}^n \cong \frac{\tau^{-\beta}}{\Gamma(2-\beta)} \sum_{s=0}^{n} b_s(u_{i,j}^{n+1-s} - u_{i,j}^{n-s})$$

where $b_s = (s+1)^{1-\beta} - s^{1-\beta}$ and $s = 0, 1, 2, \ldots n; n \geq 1$. (22)

Now (15) becomes

$$(-1)^\alpha \nabla^\alpha \cdot \left(\frac{\nabla^\alpha u_{i,j}}{\sqrt{|\nabla^\alpha u_{i,j}|^2 + \varepsilon}} \right)$$

$$+ \lambda \left(\frac{f_{i,j}}{2}(1 + e^{u_{i,j}} - f_{i,j}^2 e^{-u_{i,j}}) + 1 \right)$$

(23)

$$\frac{\tau^{-\beta}}{\Gamma(2-\beta)}(u_{i,j}^{n+1} - u_{i,j}^n) + \frac{\tau^{-\beta}}{\Gamma(2-\beta)} \sum_{s=1}^{n} b_s(u_{i,j}^{n+1-s} - u_{i,j}^{n-s})$$

$$= (-1)^\alpha \nabla^\alpha \cdot \left(\frac{\nabla^\alpha u_{i,j}}{\sqrt{|\nabla^\alpha u_{i,j}|^2 + \varepsilon}} \right)$$

$$+ \lambda \left(\frac{f_{i,j}}{2}(1 + e^{u_{i,j}} - f_{i,j}^2 e^{-u_{i,j}}) + 1 \right)$$

(24)

$$u_{i,j}^{(n+1)} = u_{i,j}^{(n)} - \sum_{s=1}^{n} b_s(u_{i,j}^{(n+1-s)} - u_{i,j}^{(n-s)}) + \Gamma(2-\beta)\tau^\beta$$

$$\times \left[(-1)^\alpha \left\{ \overline{\nabla}_x^\alpha \cdot \left(\frac{\nabla_x^\alpha u_{i,j}^{(n)}}{\sqrt{|\nabla^\alpha u_{i,j}^{(n)}|^2 + \varepsilon}} \right) \right. \right.$$

$$\left. + \overline{\nabla}_y^\alpha \cdot \left(\frac{\nabla_y^\alpha u_{i,j}^{(n)}}{\sqrt{|\nabla^\alpha u_{i,j}^{(n)}|^2 + \varepsilon}} \right) \right\}$$

$$\left. + \lambda \left(\frac{f_{i,j}}{2}(1 + e^{u_{i,j}^{(n)}} - f_{i,j}^2 e^{-u_{i,j}^{(n)}}) + 1 \right) \right]$$

(25)

Moreover to improve the process of noise removal and preserving more image details, we apply an idea to produce the modified degraded image by feed more edges and textures back to the corrupted image. Accordingly, we can get an additive residual image $f - u^{(n)}$, once obtain a noise free image $u^{(n)}$. Therefore, for the subsequent iteration stage, an advanced image $G^{(n)}$ is generated by adding the weighted image $\omega^{(n)}(f - u^{(n)})$ to the given degraded image f, which is $G^{(n)} = f + \omega^{(n)}(f - u^{(n)})$, where $\omega^{(n)}$ is referred to as the weighting matrix, $u^{(0)} = f$ and $\omega^{(0)} = 1$ (the matrix of ones). Note, here we can adopt different weighting matrix according to the given data fitting term. To obtain better restoration results and image details, we choose adaptively the parameters $\alpha_{i,j}$ and $\lambda_{i,j}$ as

$$\alpha_{i,j} = \Xi_E(i,j) + 1.7\,\Xi_T(i,j) + \Xi_F(i,j)$$

$$\times \left[\frac{1.3(P_{i,j}^{\text{pre}} - P_{Fmax}^{\text{pre}})}{P_{Fmin}^{\text{pre}} - P_{Fmax}^{\text{pre}}} + \frac{1.7(P_{i,j}^{\text{pre}} - P_{Fmin}^{\text{pre}})}{P_{Fmax}^{\text{pre}} - P_{Fmin}^{\text{pre}}} \right]$$

(26)

$$\lambda_{i,j}^{(n)} = \frac{1}{\sigma^2 N^2} \sum_{k,l=1}^{N} \left| \frac{2e^{u_{k,l}^{(n)}}(G_{k,l}^{(n-1)} - e^{u_{k,l}^{(n)}})}{f_{k,l}(2u_{k,l}^{(n)} + e^{2u_{k,l}^{(n)}} - f_{k,l}^2)} \right|$$

(27)

where $P_{Fmin}^{\text{pre}} = \min\limits_{1 \leq i,j \leq N} \{P_{i,j}^{\text{pre}} | \Xi_F(i,j) \neq 0\}$, $P_{Fmax}^{\text{pre}} = \max\limits_{1 \leq i,j \leq N} \{P_{i,j}^{\text{pre}} | \Xi_F(i,j) \neq 0\}$, σ^2 is the noise variance, N^2 is the image size and $P_{i,j}^{\text{pre}}$ is the local variance of the residual image at pixel (i,j). Hence, (25) can be reformulated as follows

$$u_{i,j}^{(n+1)} = u_{i,j}^{(n)} - \sum_{s=1}^{n} b_s(u_{i,j}^{(n+1-s)} - u_{i,j}^{(n-s)}) + \Gamma(2-\beta)\tau^\beta$$

$$\times \left[(-1)^\alpha \left\{ \overline{\nabla}_x^\alpha \cdot \left(\frac{\nabla_x^\alpha u_{i,j}^{(n)}}{\sqrt{|\nabla^\alpha u_{i,j}^{(n)}|^2 + \varepsilon}} \right) \right. \right.$$

Algorithm 1 Algorithim for SIGDS

1. Input the given noisy image f, the parameters $\varepsilon = 10^{-5}$, $\tau > 0 \; \lambda > 0, \; \beta \in (0, 1)$
2. Initialized value $u^{(0)} = f$ and $\omega^{(0)} = 1$, for $n = 1, 2, 3, \ldots$;
3. Calculate modified degraded image $G^{(n)} = f + \omega^{(n)}(f - u^{(n)})$;
4. Calculate $u^{(n+1)}$ according to (28);
5. Check if $\frac{\|\hat{u} - u\|^2}{\|u\|^2} \leq Tol$; then stop;
6. Update the weight matrix $\omega^{(n)}$ as follows;

$$\omega_{i,j}^{(n)} = \Xi_F(i,j)[c_1 + c_2]$$
$$+ \Xi_E(i,j)[c_2 + c_3] + \Xi_T(i,j)[c_3 + c_4] - 1 \quad (29)$$

here, the parameters c_1, c_2, c_3, c_4 are defined by,

$$c_1 = max\{0.7, \frac{P_{min}^{pre}}{P_{Fmean}^{pre}} c_0\},$$
$$c_2 = c_0,$$
$$c_3 = min\{1.9, (\frac{P_{Tmean}^{pre}}{P_{Fmean}^{pre}})^{1.5} c_0\},$$
$$c_4 = min\{1.9, (\frac{P_{max}^{pre}}{P_{Fmean}^{pre}})^2 c_0\}$$

with

$$c_0 = max\{0.05, 1 - e^{-\frac{0.01}{\alpha^2}}\},$$

where, $P_{min}^{pre} = \min\limits_{1 \leq i,j \leq N}\{P_{i,j}^{pre}\}$, $P_{max}^{pre} = \max\limits_{1 \leq i,j \leq N}\{P_{i,j}^{pre}\}$ and

$$P_{Fmean}^{pre} = \max\limits_{1 \leq i,j \leq j}\{P_{i,j}^{pre} | \Xi_F(i,j) \neq 0\},$$
$$P_{Tmean}^{pre} = \max\limits_{1 \leq i,j \leq j}\{P_{i,j}^{pre} | \Xi_T(i,j) \neq 0\}$$

and then denote $n = n + 1$ and go to step-3;
7. Outcome result $z = z_{\beta_1}^{(n+1)}$.

$$+ \overline{\nabla}_y^\alpha \cdot \left(\frac{\nabla_y^\alpha u_{i,j}^{(n)}}{\sqrt{|\nabla^\alpha u_{i,j}^{(n)}|^2 + \varepsilon}} \right) \}$$

$$+ \lambda_{i,j}^{(n)} \left(\frac{G_{i,j}^{(n)}}{2}(1 + e^{u_{i,j}^{(n)}} - G_{i,j}^{2(n)} e^{-u_{i,j}^{(n)}}) + 1 \right) \right] \quad (28)$$

The numerical solutions of $u_{i,j}^{(n+1)}$ and $u_{i,j}^{(n)}$ are defined from the given initial and symmetric boundary conditions (19). In order to get $u_{i,j}^{(n+1)}$, the right hand side computation of (28) should be performed. The solution $u_{i,j}^{(n+1)}$ of (28) is represented as a denoised image with better PSNR and SSIM values. To conclude, the iterative method is performed in the steps given as follows.

V. EXPERIMENTAL RESULTS AND ANALYSIS

Some image restoration outcomes are given in this part of the paper to confirm the achievement of the suggested model M1 and a fast algorithm for its numerical solution. The numerical results are contrasted with the schemes for M2, M3, and M4. In this experiments, multiplicative noise carrying a Gamma distribution with a mean one and Rayleigh

distribution (i.e. with error variation $\sigma^2 = [0.01 - 0.3]$ and the number of looks $L = 5$) contaminates the image provided. The suggested model is applied to various images containing (two synthetic, eight natural, five medical, and six SAR) of size $[256^2 - 512^2, 1820 \times 720]$ respectively. The values of α and λ are tuned adaptively according to the image type and size. It is noted that $\alpha \in [1, 2]$ and $\lambda \in [0.5, 5000]$ according to image type and size. The adapted values of α and λ are displayed in the figures given below. All simulations reported here are implemented in MATLAB-R2013a and all analyzes have been conducted on Intel(R) Core(TM) i5-3230M CPU @2.60GHz 2.60GHz, 4.00Gb RAM and 64-bit operating system. In this article, two methods to test the outcomes of denoising are considered. The first is the peak signal to noise ratio PSNR (dB) for measuring the quality of the picture. This measure can be formulated as

$$PSNR(db) = 10log_{10}\left[\frac{m^2}{\frac{1}{N \times N}\sum\limits_{i=1}^{N}\sum\limits_{j=1}^{N}(\hat{u} - u)^2} \right] \quad (30)$$

The other is the structural similarity index (SSIM), which measures the structural detail similarity between u and $\hat{u}$. The SSIM is defined by

$$SSIM(u, \hat{u}) = \frac{(2\mu_{\hat{u}}\mu_u)(2\sigma_{\hat{u}u} + a_2)}{(\mu_{\hat{u}}^2 + \mu_u^2 + a_1)(\sigma_{\hat{u}}^2 + \sigma_u^2 + a_2)} \quad (31)$$

where μu and μu are the mean measurements of images u and $\hat{u}$, σu and σu indicate their standard deviations, and σu is the co-variance of u and $\hat{u}$. Furthermore, $a1 = (0.01d)^2$ and $a2 = (0.03d)^2$ are carried, where d is the dynamic range (255 for 8-bit grayscale images). The SSIM value range is [0, 1] with one value for the ideal standard. CPU time(s) used by these algorithms to determine the numerical efficacy of the algorithms under consideration after the iterations are finished. For all the numerical schemes, we utilize the alike end condition as under

$$\text{Relative Error} = \frac{\|\hat{u} - u\|^2}{\|u\|^2} \leq [10^{-4}, 10^{-6}] \quad (32)$$

where m is the image's biggest pixel value, u is the real picture, and $\hat{u}$ is the denoted image.

A. SYNTHETIC IMAGES

We first approximate the effectiveness of the suggested model (M1) utilizing two synthetic images with a scale of 256^2 and 512^2. The images are distorted by multiplying noise with noise variances $\sigma^2 = 0.03$ and 0.2 separately. The reconstruction outcomes in Fig.1 and Fig.2 show that the suggested approach seems to preserve the image features effectively and thereby provides images that look more natural. In addition, the appropriate PSNR (dB), SSIM, relative error, number of iteration steps and CPU time(s) results in Fig.1, Fig.2 and Table.1 demonstrate that our approach performs improved latent (denoising) images reliably and efficiently. It is also noted that the proposed model retains image edges, textures and does not create artifacts along the edges.
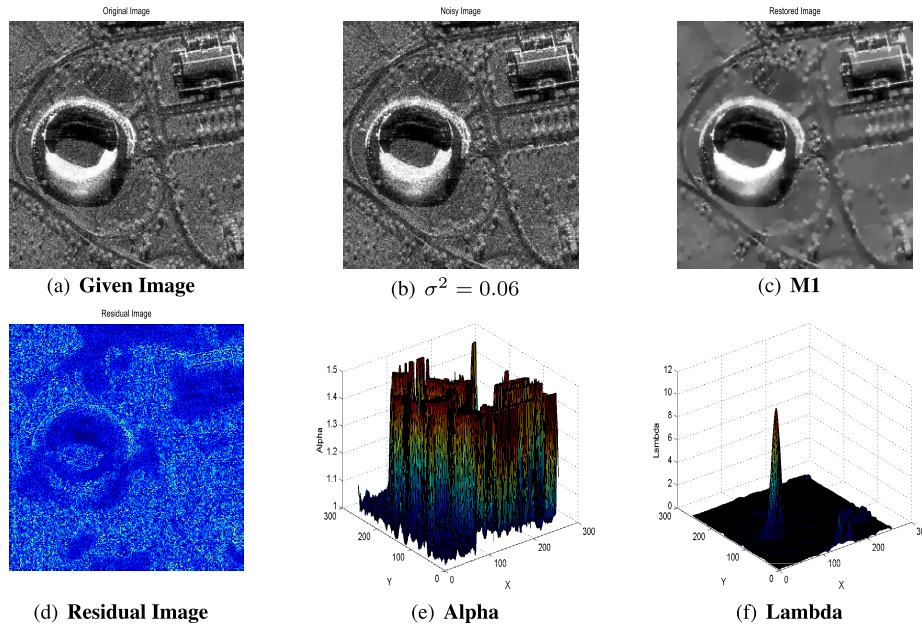
(a) **Given Image**   (b) $\sigma^2 = 0.06$ (c) **M1**

(d) **Residual Image**   (e) **Alpha**   (f) **Lambda**

FIGURE 11. a) Given image 256^2; b) Degrade image with $\sigma^2 = 0.06$; c) De-noised image; d) Residual image; e) Adaptive value of α; f) Adaptive value of λ respectively.

TABLE 4. Performance of the proposed model (M1) on SAR images of size (256^2) and corrupted by multiplicative noise of variance $\sigma^2 = 0.08$ and 0.06 in terms of ENL(A), ENL(B), ENL(C) and EPI results.

Problem	σ^2/L	image size	Proposed Model (M1)			
			ENL(A)	ENL(B)	ENL(C)	EPI
Fig.10	0.08	256^2	118.5818	157.5047	307.0471	0.8716
Fig.11	0.06	256^2	10.8584	10.6624	2.4023	0.8663

B. REAL-WORLD IMAGES

To prove further the better performance of the proposed model qualitatively and quantitatively, in Fig.3–8, we present denoising results for natural images with size range from 256^2 to 1820×720. The images are degraded with different noise variance levels $\sigma^2 = 0.02, 0.2, 0.3$ and $L = 5$. The corresponding PSNR (db), SSIM, relative error, iteration steps and computational time results are also displayed in Table. 2 and Figs.3(g,h, i)–8 (g,h,i), respectively. Adaptive automatically tuned values of α and λ are shown in Figs. 3(e,f)–8 (e,f). Our recovered results subtle image features while at the same time avoids staircase artifacts successfully. Overall, our method can obtain better restoration outputs with optimal PSNR (db), SSIM, relative error results and computational CPU costs respectively.

C. MEDICAL IMAGES

This section focuses on testing denoising potential of the proposed model (M1) on three MRI (brain and kidney) medical images. The images having size 256^2 are contaminated with different noise variance levels $\sigma^2 = 0.08, 0.1$ and $L = 5$, for details see Figs.7, 8, and 9. The adaptive values of α and λ can be observed from Figs. 7(e,f), 8(e,f), and 9(e,f). The residual image results in Figs. 7(d), 8(d), and 9(d) show that the model (M1) can preserve image edges, textures

and other features quite well. The output results in Table.3, Figs. 7(c,g,h,i), 8(c,g,h,i), and 9(c,g,h,i) demonstrate that the proposed method (M1) produces images that look more natural, reduces staircase artifacts effectively and give optimal PSNR, SSIM, relative error and CPU time (s) values.

D. SAR IMAGES

Furthermore, in order to test the ability of model M1 for multiplicative noise (speckle) removal, several tests have been carried out on true SAR-images (where the noise is supposed to support Gamma distribution) (where the noise is supposed to support Gamma distribution). The results are seen in Figs.10, 11, 12, and 13. As in Figs.10-11, the indicated (clean) image is not recognized, so the related PSNR and SSIM values cannot be evaluated. In this case, we use the same number of looks (ENL) and the Edge-Preserving Index (EPI) as the criterion for scientific evaluation. Large ENL means a greater opportunity for noise removal in flat areas, and a larger EPI infers better edge conservation efficiency. The ENLs are evaluated in the regions ENL(A)(10, 50, 50, 120), ENL(B)(85, 125, 135, 185), and ENL(C)(130, 160, 25, 60). The results are shown in Figs.10(c)-11(c) and the computed indexes in Table.4. Outputs have shown that the proposed approach can provide an optimal high (EPI and ENL) with low computational
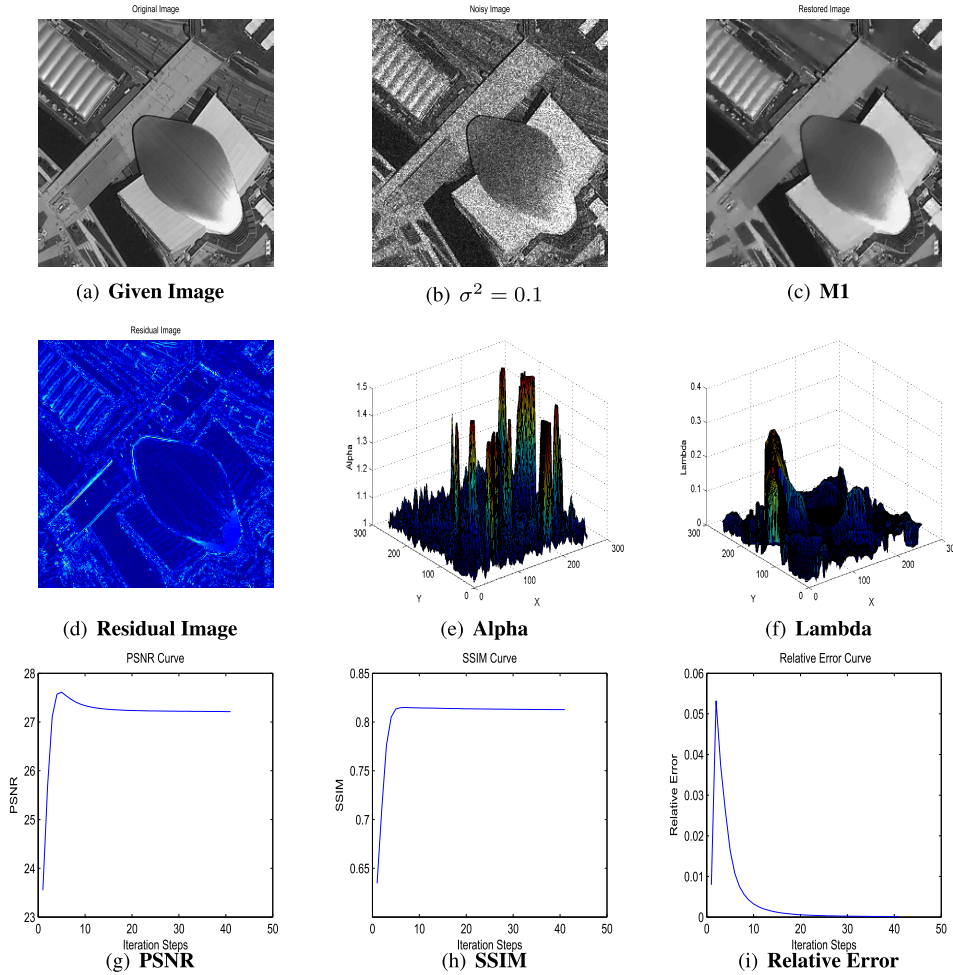
FIGURE 12. a) Given image 256^2; b) Noisy image with $\sigma^2 = 0.1$; c) De-noised image; d) Residual image; e) Adaptive value of α; f) Adaptive value of λ; g) PSNR result; h) SSIM result; i) Relative error result with number of iteration steps respectively.

TABLE 5. Achievement of the proposed model (M1) on SAR images of size (256^2) and corrupted by multiplicative noise of variance $\sigma^2 = 0.1$, and 0.2 regarding PSNR (db), SSIM, relative error and CPU time (s) results.

Problem	σ^2/L	image size	Proposed Model (M1)			
			PSNR (db)	SSIM	Relative Error	CPU Time (s)
Fig.12	0.1	256^2	27.21	0.8127	0.005	6.14
Fig.13	0.2	256^2	26.23	0.7612	0.00043	7.85

time and can preserve edges and textures showed by residual images in Figs.10(d)–11(d).

In Figs.12–13, the real SAR images having size 256^2 are contaminated by speckle with different noise variance $\sigma^2 = 0.1, 0.2$. From the restoration results given in Figs.12–13 and the PSNR, SSIM, relative error and CPU time values given in Table.5 and Figs.12(g,h,i)–13(g,h,i), one can check that the proposed method (M1) is able to get better de-noised images and recover smooth regions, avoiding staircase effects as well as discontinuous at object boundaries.

E. COMPARISON TO PREVIOUS DE-NOISING METHODS
In this portion, we present some experimental findings to demonstrate the effectiveness and potential of the suggested

model (M1). The outputs obtained are confronted with those of the FLG-model (M2) [41], the HMW-model (M3) [42] and the DRS-model (M4) [43].

1) FLG-MODEL (M2)
Using the MAP estimation technique of MAP, W. Feng *et al.* [41] recommended a variational model based on $TGV\gamma^2$ to remove multiplicative noise is given by

$$u^\star = arg \min_u \left\{ \alpha_1 \int_{\Omega_0} (u + fe^{-u})dxdy + TGV_\gamma^2(u) \right\},$$
$$\text{with } u^\star_{final} = e^{u^\star} \quad (33)$$

where the first term is the data fitting term which is derived from MAP and α_1 is the regularization parameter. TGV_γ^2 as

(a) **given Image**

(b) $\sigma^2 = 0.2$

(c) **M1**

(d) **Residual Image**

(e) **Alpha**

(f) **Lambda**

(g) **PSNR**

(h) **SSIM**

(i) **Relative Error**

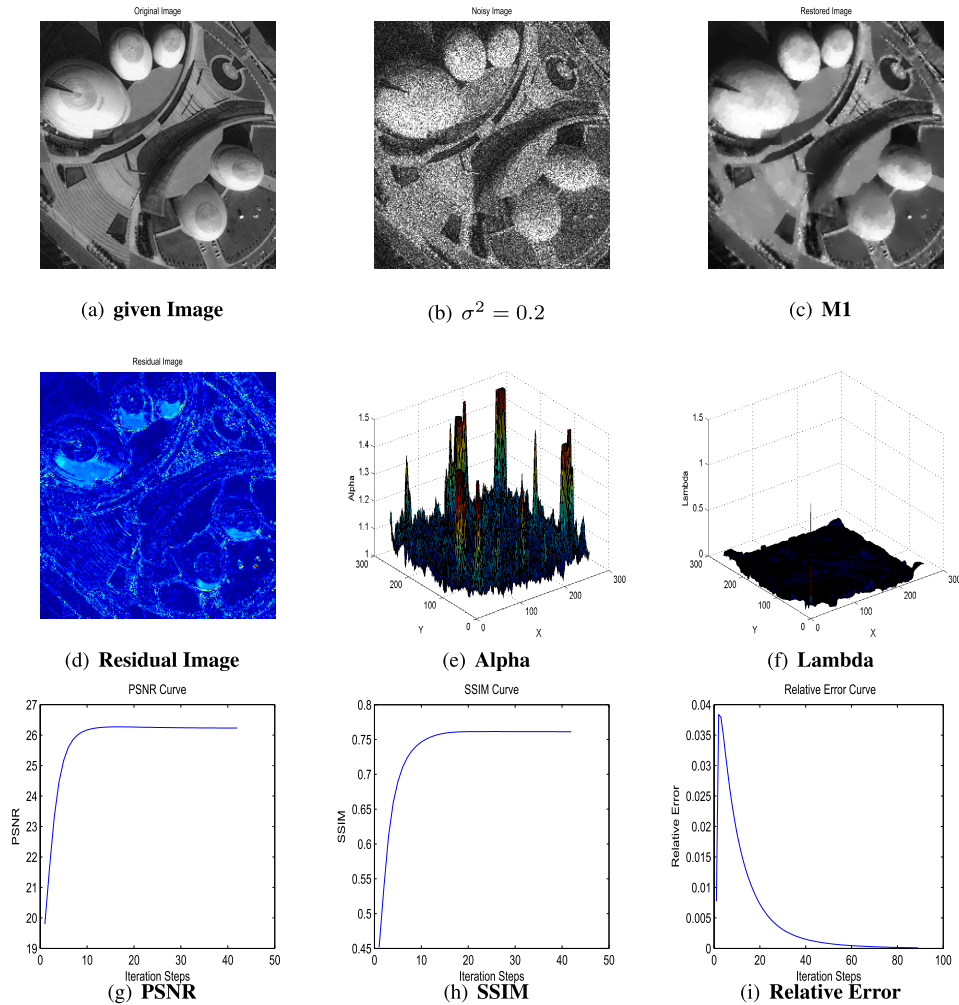**FIGURE 13.** a) Given image 256^2; b) Contaminated image with $\sigma^2 = 0.2$; c) De-noised image; d) Residual image; e) Adaptive value of α; f) Adaptive value of λ; g) PSNR result; h) SSIM result; i) Relative error result with number of iterations respectively.

defined in (34) is the regularization term.

$$TGV_\gamma^2(u) = \min_{v \in V} \gamma_1 \|\nabla u - v\|_1 + \gamma_0 \|\bar{\varepsilon}(v)\|_1 \quad (34)$$

primal-dual algorithm was employed to compute minimizer of (33). For more details, the interested reader is refereed to [41].

2) HNW-MODEL (M3)

By using the alternating minimization algorithm [12], the numerical solution of the HMW-model is computed as under.

$$\min_{z,w} = \Bigg[\sum_{i,j=0}^{N \times N} \left(z_{i,j} + f_{i,j} e^{-z_{i,j}} \right)$$
$$+ \alpha_1 |z_{i,j} - w_{i,j}|_2^2 + \alpha_2 TV(w_{i,j}) \Bigg] \quad (35)$$

where the parameters α_1, α_2 and the stopping criterion of the HMW model (M3) are selected as suggested in [42].

3) DRS-MODEL (M4)

Applying the MAP approach, Steidl *et al.* [43] considered the following convex image restoration model as

$$u^\star = \arg \min_{u \in BV, u>0} \left\{ \int_\Omega (\text{u-f } logu)dxdy + \gamma \int_\Omega |\nabla u| dxdy \right\} \quad (36)$$

where the data fitting term is shown by the first term, while the regularization parameter is γ and the second term is known as the total variational regularizer. The minimizer of the energy functional is computed by employing the Douglas-Rachford splitting methods. For more details see [43].

4) PGD-MODEL (M5)

Thanh et.al suggested the new TV-based scheme [44] to remove the mixed Poisson-Gaussian noise from the images. The functional for this scheme is given as under.

$$L(u, \tau) = \int_\Omega |\nabla u| dxdy + \tau \left\{ \frac{\lambda_1}{2\sigma_2} \int_\Omega (v - u)^2 dxdy \right.$$
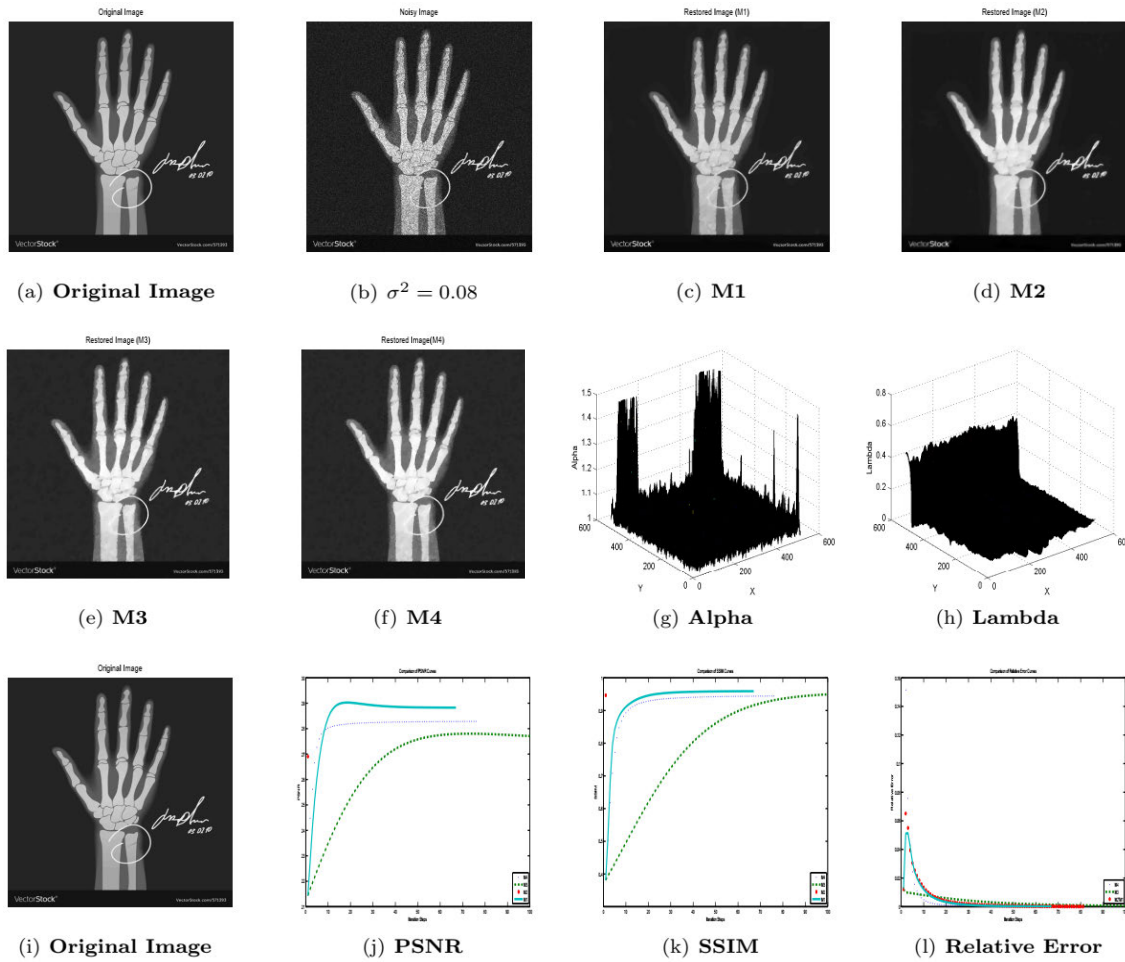
FIGURE 14. a) True image 512^2; b) Degraded image with $\sigma^2 = 0.08$; denoised image c) M1; d) M2; e) M3; f) M4; g) Adaptive value of α; h) Adaptive value of λ; i) Original image; comparison of the performance of M1, M2, M3 and M4 methods with j) PSNR; k) SSIM and l) Relative error results respectively.

$$+\lambda_2 \int_\Omega (u - v \ln(u)) dx dy - k \Big\}, \quad (37)$$

where τ is known as Lagrange multiplier. Here, $\lambda_1 > 0$ and $\lambda_2 > 0$. The solution of (37) result in the given Euler-Lagrange equation.

$$\frac{\lambda_1}{\sigma^2}(v - u) + \lambda_2\left(1 - \frac{v}{u}\right) - \mu \frac{\partial}{\partial x}\left(\frac{u_x}{\sqrt{u_x^2 + u_y^2}}\right)$$
$$-\mu \frac{\partial}{\partial y}\left(\frac{u_x}{\sqrt{u_x^2 + u_y^2}}\right) = 0. \quad (38)$$

The Lagrange multipliers method have been utilized to solve equation (38). For more information, the readers are refereed to [44].

5) MNRNRTVWF-MODEL (M6)
Chunyan et. al proposed a model [45] for multiplicative noise removal and found some good restoration results. The model

for multiplicative noise removal is

$$\min_{u,\alpha,v} F(u, \alpha, v) =: f(u) + g(\alpha, u) + h(v, u), \quad (39)$$

where α, and v are the two auxiliary variables. Also

$$f(u) = <u, f \log u, 1>,$$
$$g(\alpha, u) = \lambda_1 \sum_{i=1}^{n_1} \varphi_1(\alpha_i) + \frac{\beta_1}{2}\|\alpha - Wu\|^2,$$

and

$$h(v, u) = \lambda_2 \sum_{i=1}^{n_2} \varphi_2(D_i v) + \frac{\beta_2}{2}\|u - v\|^2.$$

Although model (39) is yet nonconvex, the function $F(u, \alpha, v)$ is strongly convex concerning u, α, and v under some conditions. respectively. The component-wise strong convexity provides the numerical ability for solving the nonconvex problem. The authors then utilized an alternating minimization scheme to solve the problem (39). Beginning of an introductory guess u_0, then a new sequence was obtained which is
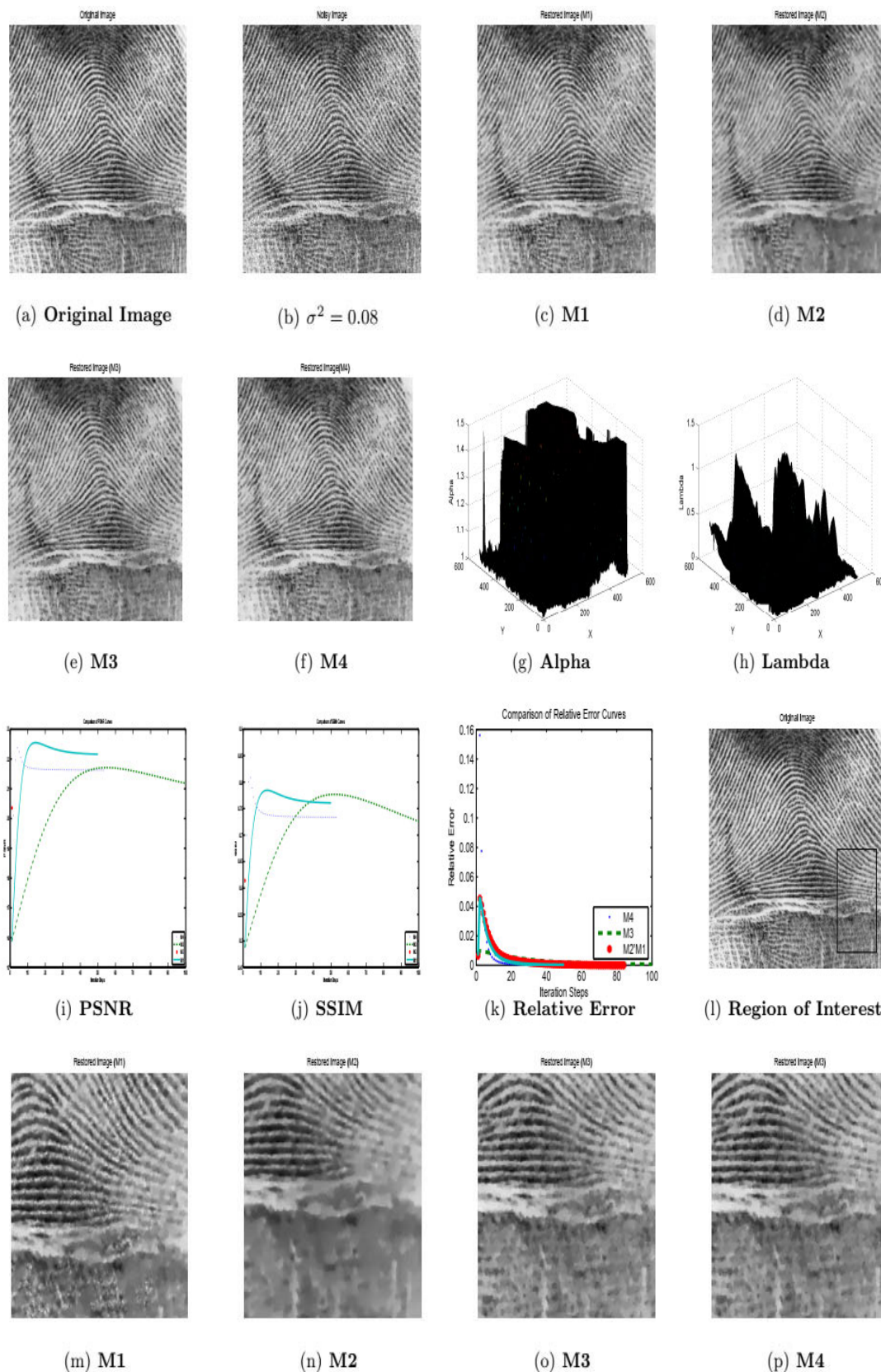
FIGURE 15. a) Original image 512^2; b) Degraded image with $\sigma^2 = 0.08$; denoised image c) M1; d) M2; e) M3; f) M4; g) Adaptive value of α; h) Adaptive value of λ; i) original image; comparison of the performance of M1, M2, M3 and M4 methods with j) PSNR; k) SSIM and l) Relative error results; restored results by m) M1; n) M2; o) M3; p) M4 respectively.

FIGURE 16. a) True image 512^2; b) Degraded image with $\sigma^2 = 0.03$; denoised image c) M1; d) M2; e) M3; f) M4; g) Adaptive value of α; h) Adaptive value of λ; comparison of the performance of M1, M2, M3 and M4 methods with i) PSNR; j) SSIM and k) Relative error results; l) Region of interest; restored result by m,q) M1; n,r) M2; o,s) M3; p,t) M4 respectively.
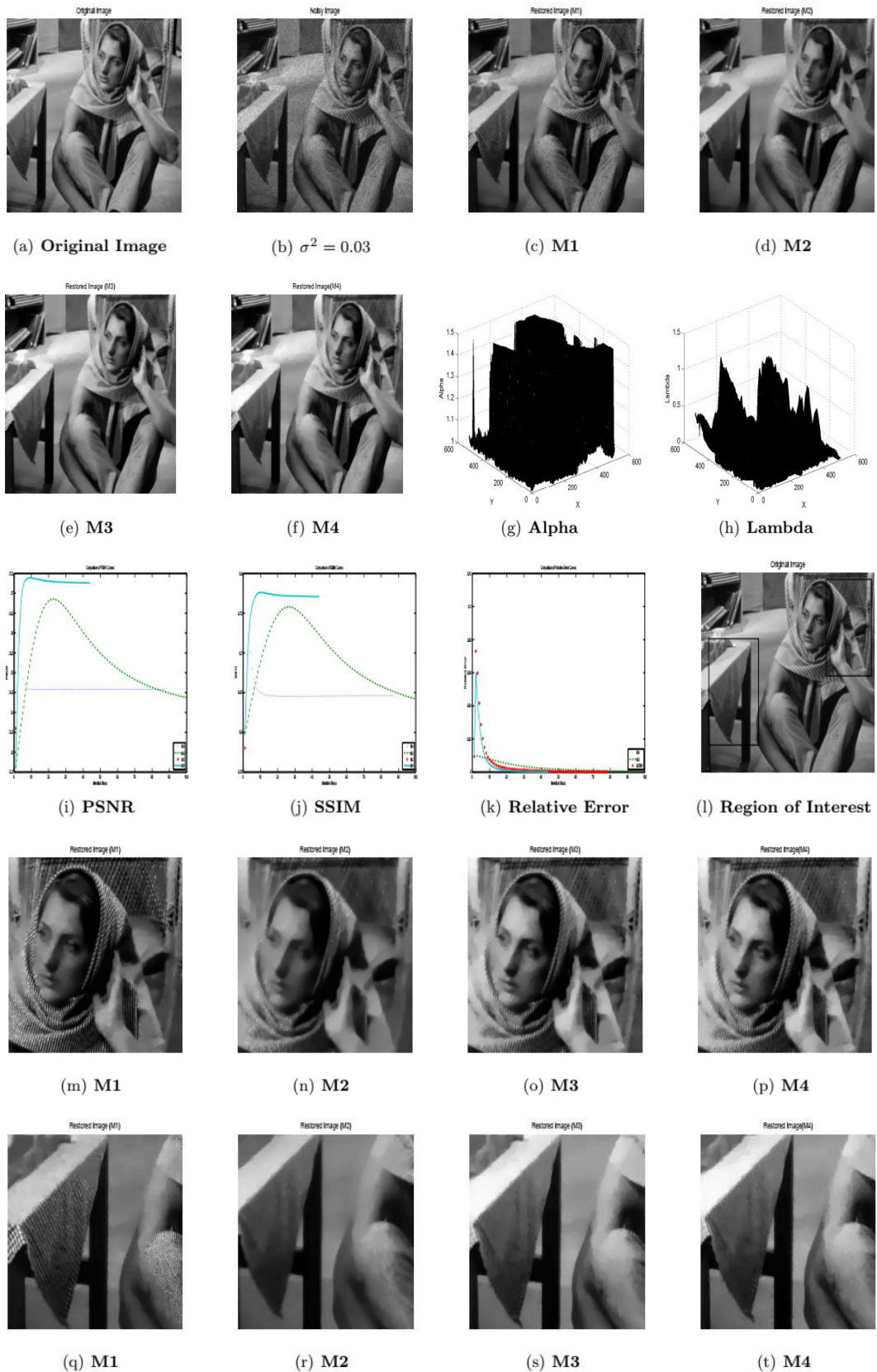
FIGURE 17. a) True image 512^2; b) Degraded image with $\sigma^2 = 0.1$; denoised image c) M1; d) M2; e) M3; f) M4; g) Adaptive value of α; h) Adaptive value of λ; comparison of the performance of M1, M2, M3 and M4 methods with i) PSNR; j) SSIM and k) Relative error results; l) Region of interest; restored result by m) M1; n) M2; o) M3; p) M4 respectively.

FIGURE 18. a) True image 512^2; b) Noisy image with $\sigma^2 = 0.03$; denoised image c) M1; d) M2; e) M3; f) M4; g) Adaptive value of α; h) Adaptive value of λ; comparison of the performance of M1, M2, M3 and M4 methods with i) PSNR; j) SSIM and k) Relative error results; l) Region of interest; restored result by m) M1; n) M2; o) M3; p) M4 respectively.
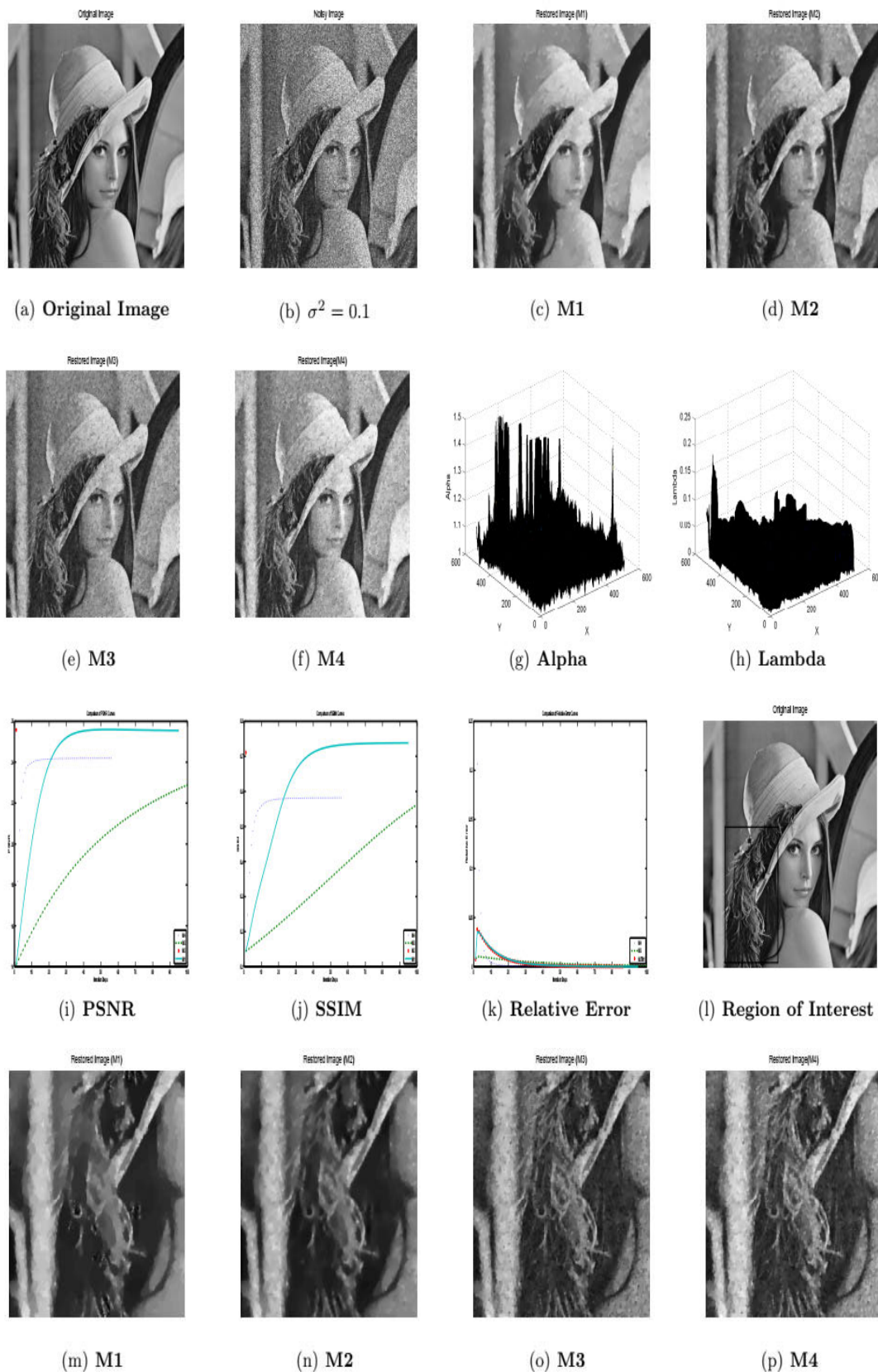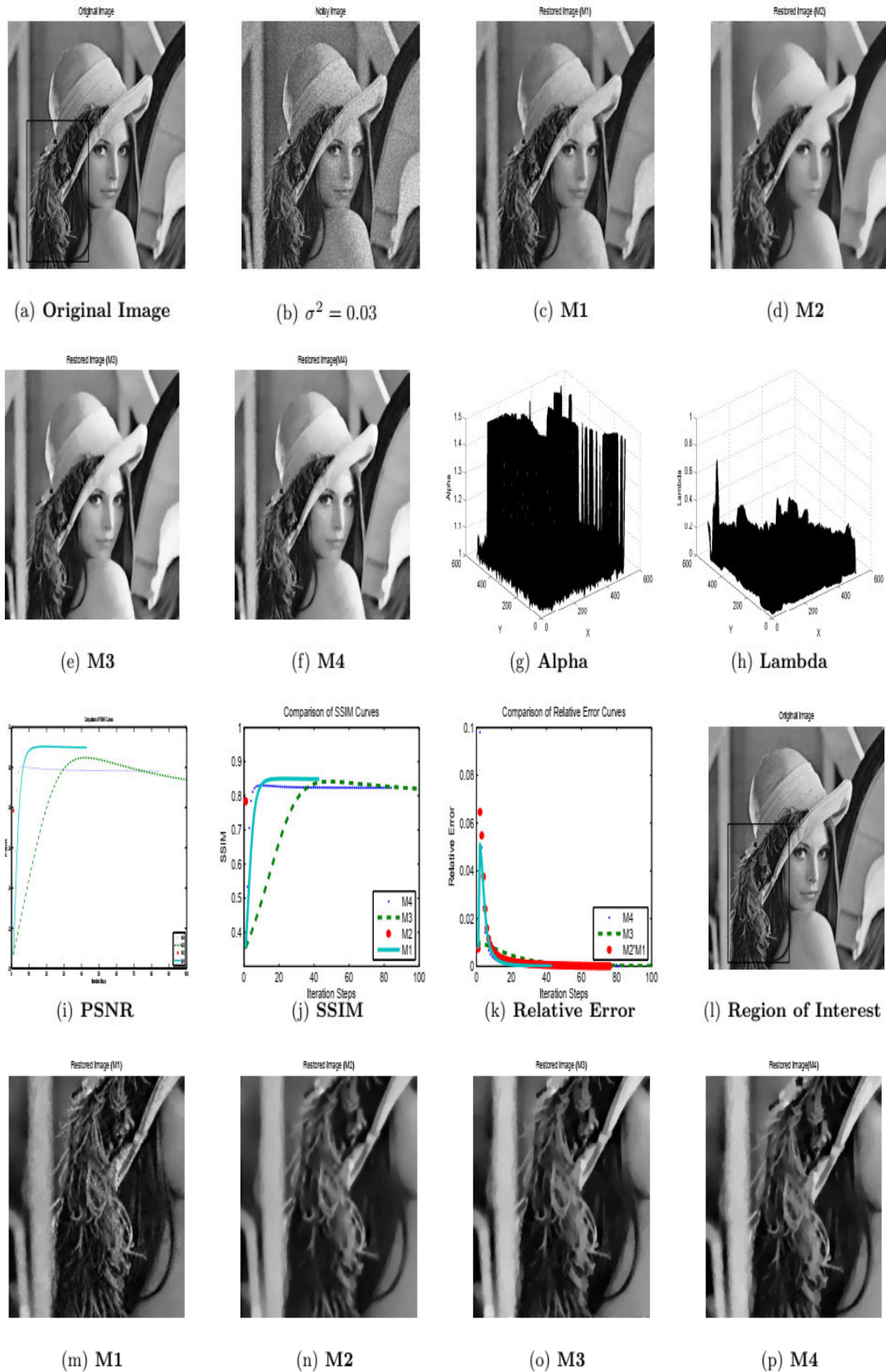
TABLE 6. Comparison of the performance of the M1, M2, M3 and M4 methods on images of size (512^2) degraded by multiplicative noise of variance $\sigma^2 = 0.08, 0.03$ and **0.1** in terms of PSNR and SSIM.

Problem	σ^2/L	image	Proposed Model (M1)		Model-M2		Model -M3		Model-M4	
			PSNR	SSIM	PSNR	SSIM	PSNR	SSIM	PSNR	SSIM
Fig.14	0.08	512^2	**28.89**	**0.9587**	26.96	0.9472	27.82	0.9155	28.33	0.9443
Fig.15	0.08	512^2	**22.16**	**0.7606**	20.35	0.6141	21.69	0.7766	21.62	0.7339
Fig.16	0.03	512^2	**27.26**	**0.7708**	23.60	0.5802	25.79	0.7231	24.58	0.6463
Fig.17	0.1	512^2	**25.55**	**0.7384**	25.57	0.7109	22.70	0.5452	24.19	0.5817
Fig.18	0.03	512^2	**30.97**	**0.8478**	27.73	0.7802	30.52	0.8395	29.83	0.8229

TABLE 7. Comparison of the performance of the methods: M1, M2, M3 and M4 on images of size (512^2) corrupted by multiplicative noise of variance $\sigma^2 = 0.08, 0.03$ and **0.1** in terms of relative error and CPU time (s).

Problem	σ^2/L	image	Proposed Model (M1)		Model-M2		Model -M3		Model-M4	
			Rel. Error	CPU	Rel. Error	CPU	Rel. Error	CPU	Rel. Error	CPU
Fig.14	0.08	512^2	**9.4e-5**	**59.63**	1e-4	6.94	1.4e-4	6.94	1e-4	6.94
Fig.15	0.08	512^2	**9.3e-5**	**43.20**	1e-4	43.20	2.1e-3	74.52	1e-4	27.38
Fig.16	0.03	512^2	**9.6e-5**	**27.38**	1e-4	39.67	2e-3	70.25	9.8e-4	54.69
Fig.17	0.1	512^2	**9.8e-5**	**54.69**	1e-4	94.41	1e-3	95.59	9.9e-4	30.64
Fig.18	0.03	512^2	**8.4e-5**	**54.69**	1e-4	94.41	1e-3	95.59	9.6e-4	30.64

given as under.

$$(u^0, \alpha^0, v^0), (u^1, \alpha^1, v^1), (u^2, \alpha^2, v^2), (u^k, \alpha^k, v^k) \ldots \ldots$$

generated by

$$
\begin{cases}
u^{k+1} = \arg\min_u < u, flogu, 1 > + \dfrac{\beta_1}{2} \|\alpha^k \\
- Wu\|^2 + \dfrac{\beta_2}{2} \|u^k - v\|^2 \\
\alpha^{k+1} = \arg\min_\alpha g(\alpha, u^{k+1}) = \lambda_1 \sum_{i=1}^{n_1} \varphi_1(\alpha_i) \\
+ \dfrac{\beta_1}{2} \|\alpha - Wu^{k+1}\|^2 \\
v^{k+1} = \arg\min_\alpha h(v, u^{k+1}) = \lambda_2 \sum_{i=1}^{n_2} \varphi_2(D_i v) \\
+ \dfrac{\beta_2}{2} \|u - v\|^2, \quad for \quad k = 1, 2, \ldots
\end{cases}
\tag{40}
$$

For further information, see [45].

6) AMRHOTVIG-MODEL (M7)

Dang et. al proposed Higher order model [46] for multiplication noise removal using the alternating directionmethod of multipliers(ADMM)and hence some effective restoration results have been obtained. The proposed model is stated as under.

$$
\arg\min_u \left\{ \int_\Omega |\nabla u|_2 dx + k \int_\Omega |\nabla^2 u|_2 dx \right.
$$
$$
\left. + \frac{\lambda(v)}{2} \int_\Omega |u - v|_2^2 dx \right\}, \tag{41}
$$

with

$$
\lambda(v) = \frac{\mu}{1 + \tau max_\rho |G_\rho \star \nabla v|_2^2},
$$

where $G_\rho = \frac{1}{2\Pi\rho^2} exp\left(-\frac{x_1^2 + x_2^2}{2\rho^2}\right)$. Including each value of scale parameter ρ, the authors obtained a similar value of expression $|G_\rho \star \nabla u|_2$. After assessing all values of $|G_\rho \star \nabla u|_2$ in all of scales ρ, they took the they took the maximum value $|G_\rho \star \nabla u|_2^2$. This value was employed for determining the

value of the regularization parameter λ in the model. The authors then used the alternating directionmethod of multipliers(ADMM) to solve (41). For further details, see [46].

7) EXAMPLE-01

Two medical images namely the X-ray and fingerprint images of size 512^2 are degraded with multiplicative noise of noise variance $\sigma^2 = 0.08$ are utilized as test images. The main concept of the model (M1) is to exploit the benefit of the FOTV regularizer and the fuzzy membership degrees to obtain images that look more natural. In Figs.14 and 15, we compared the de-noising results of the M2-model, M3-model, and M4-model with the recommended model (M1). The model (M1) yields better restoration results comparing to other methods since it preserves edges, textures, and other fine details whereas at the same time decreasing the blocky effect as well. The α and λ adaptive parameters are described in Fig14(g,h)–15(g,h). Furthermore, the results are given in Tables. 6–7, and Figs.14(j,k,l)– 15(i,j,k), clarify that the method (M1) delivers better PSNR, SSIM and relative error values of restored images compared t]o other methods.

8) EXAMPLE-02

The Barbara and Lena images of size 512^2 with noise variance $\sigma^2 = 0.03, 0.1$ are used as test images. In Fig.16–Fig.18, we present the recovered pictures, flat sections, and texture sections achieved by applying (the M1, M2, M3, and M4) models. The comparing PSNR, SSIM. relative error and CPU time results are also mentioned in Figs.16(i,j,k)–18(i,j,k) and Tables.6–7. The adaptive tuned values of α and λ are also showed in Figs.16(g,h)–18(g,h). In particular, the black color rectangles showed in Figs.16(l)–18(l) indicate segments of specific concern in every scene which are zipped in Fig.16(m,n,o,p,q,r,s,t), Figs.17(m,n,o,p) and 18(m,n,o,p), in order to display the better results of the potential model (M1) comparing
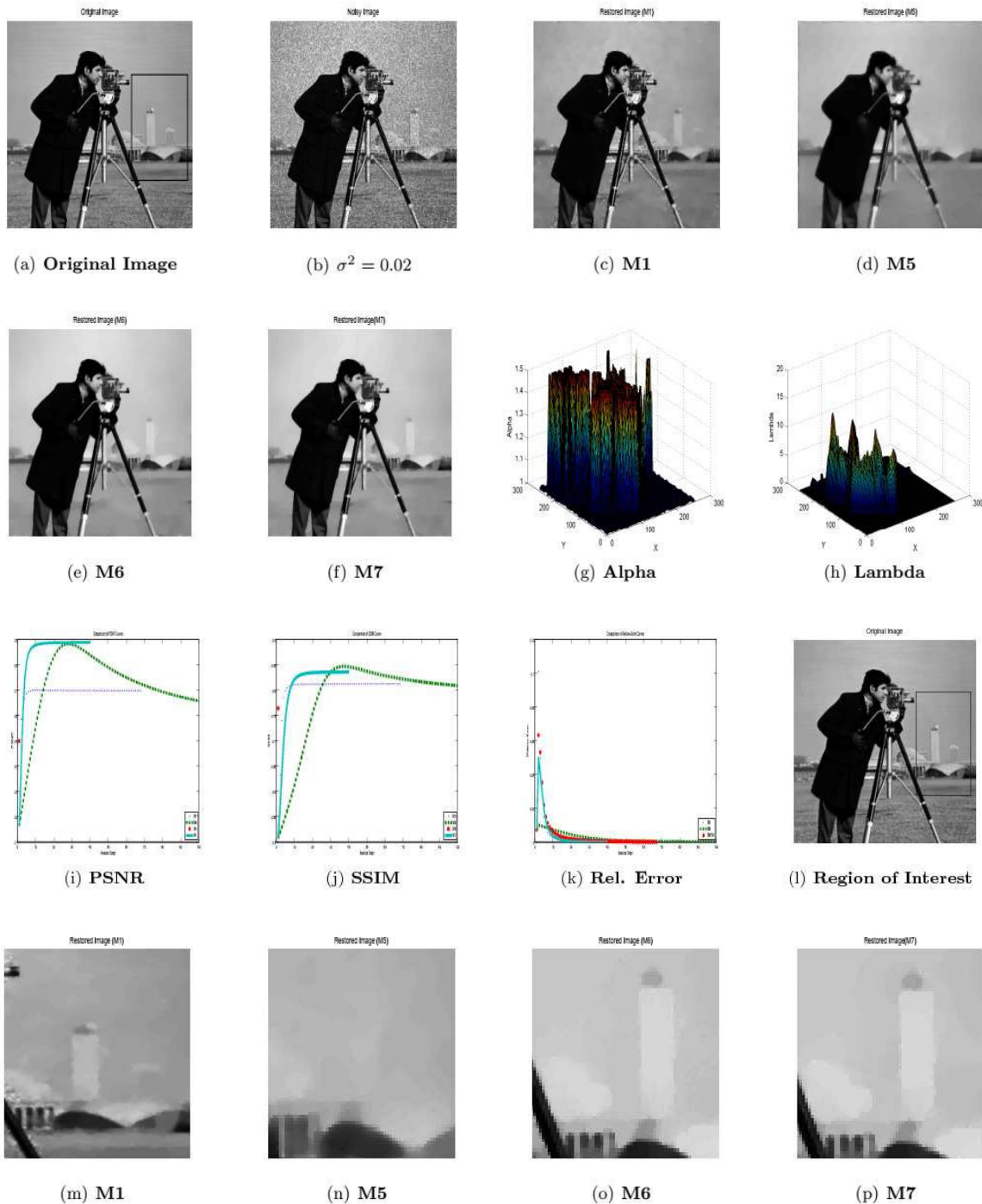
FIGURE 19. a) original image 256^2; b) noisy image with $\sigma^2 = 0.02$; denoised image c)M1; d)M5; e) M6; f) M7; g)adaptive value of α; h) adaptive value of λ; comparison of the performance of M1, M5, M6 and M7 methods with i) PSNR; j) SSIM and k) relative error results; l) region of interest; restored result by m) M1; n) M5; o) M6; p) M7 respectively.

to other competing methods. The findings shown in Figs.16(c,d,e,f)–18(c,d,e,f) and Tables.6–7 clearly demonstrates that the suggested model (M1) retains sharp edges, textures and at the same time minimizes the blocky effect better than FLG-model (M2) [41], the HMW-model (M3) [42] and the DRS-model (M4) [43]. Furthermore, the numerical

outputs in Table. 6–7 demonstrate that the model (M1) can efficiently improve the PSNR, SSIM, relative error of recovered images better than compared to other schemes. Therefore, it is fair to conclude that the model (M1) is better than other models in the sense that it has sharp edges, piecewise smooth intensities and reduces the blocky effect.
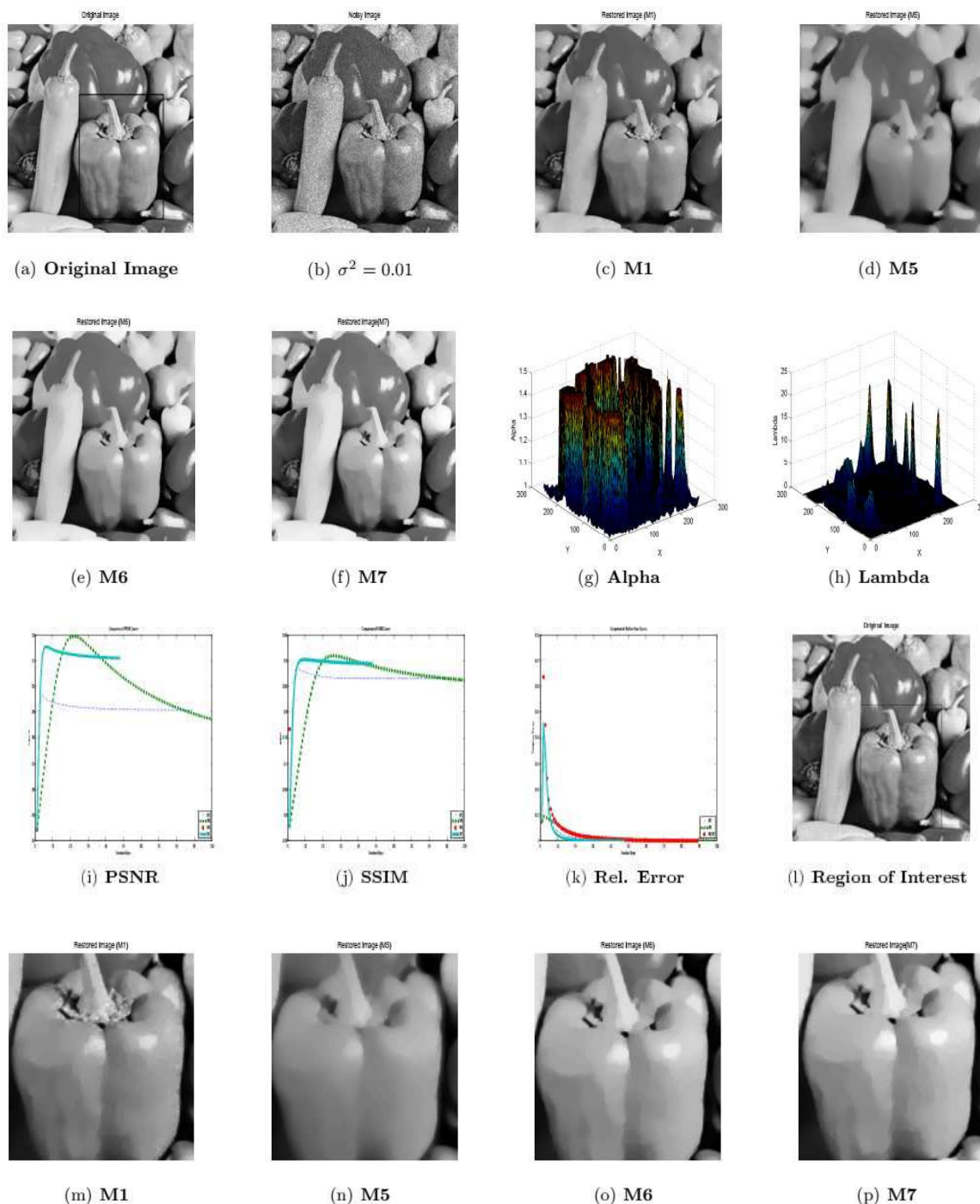
FIGURE 20. a) original image 256^2; b) noisy image with $\sigma^2 = 0.01$; denoised image c)M1; d)M5; e) M6; f) M7; g)adaptive value of α; h) adaptive value of λ; comparison of the performance of M1, M5, M6 and M7 methods with i) PSNR; j) SSIM and k) relative error results; l) region of interest; restored result by m) M1; n) M5; o) M6; p) M7 respectively.

TABLE 8. Comparison of the performance of the M1, M5, M6 and M7 methods on images of size (256^2) degraded by multiplicative noise of variance $\sigma^2 = 0.02, 0.01$ in terms of PSNR and SSIM.

Problem	σ^2/L	image	Proposed Model (M1)		Model-M5		Model -M6		Model-M7	
			PSNR	SSIM	PSNR	SSIM	PSNR	SSIM	PSNR	SSIM
Fig.19	0.02	256^2	**28.89**	**0.84**	24.98	0.76	28.39	0.83	26.98	0.81
Fig.20	0.01	256^2	**31.09**	**0.90**	24.46	0.77	30.44	0.88	29.76	0.86

TABLE 9. Comparison of the performance of the methods: M1, M5, M6 and M7 on images of size (256^2) corrupted by multiplicative noise of variance $\sigma^2 = 0.02, 0.01$ in terms of relative error and CPU time (s).

Problem	σ^2/L	image	Proposed Model (M1)		Model-M5		Model -M6		Model-M7	
			Rel. Error	CPU	Rel. Error	CPU	Rel. Error	CPU	Rel. Error	CPU
Fig.19	0.02	256^2	**9.2e-5**	**8.75**	1.4e-4	13.95	1e-4	6.42	1e-5	9.58
Fig.20	0.01	256^2	**8.3e-5**	**9.61**	1e-4	14.3	7.1e-3	8.23	1.2e-4	9.61

9) EXAMPLE-03

The Cameraman and Pepper images of size 256^2 with noise variance $\sigma^2 = 0.02, 0.01$ are selected as test objects. In Figs.19–20, we present the restored images, flat regions and texture regions achieved by applying (the M1, M5, M6 and M7) models. The comparing PSNR, SSIM. relative error and CPU time outputs are also shown in Figs.19(i,j,k)–20(i,j,k) and Tables.8–9. The adaptive tuned values of α and λ are also mentioned in Figs.19(g,h)–20(g,h). In particular, the black color rectangles showed in Figs.19(l)–20(l) indicate segments of special interest in each scene which are zoomed in Figs.19(m,n,o,p) and 20(m,n,o,p), in order to show the results of the potential model (M1) comparing to other competing methods. The results shown in Figs.19(c,d,e,f)–20(c,d,e,f) and Tables.8–9 clearly demonstrate that the proposed model (M1) yields better restoration results since it preserves sharp edges, textures and at the same time reduces the staircase effect better than M5, M6 and M7. Furthermore, the numerical results in Tablse.8–9 demonstrate that the model (M1) can efficiently improve the PSNR, SSIM, relative error of recovered images better than compared to other methods. Hence, it is concluded that the model (M1) is best in the sense that it has sharp edges, piecewise smooth intensities, and minimizing the staircase effect better than other models.

VI. CONCLUSION AND FUTURE WORK

In this article, a new fractional-order (space and time) total variation regularized model for multiplicative noise removal is introduced and develop a semi-implicit gradient descent numerical algorithm for computing its numerical solution. To develop the proposed model better performance, the changing fuzzy membership degrees are defined gradually to characterize the likelihood of a pixel relating to edges, textured and flat regions, and hence this strategy performs well for reducing the fragmenting effect. Through several examples, we showed that the proposed model produces optimal results over other methods. Experimental outcomes (on synthetic, natural, medical, and SAR images) showing the better potential of our method than other methods in preserving edges, textured regions, flat regions, and eliminating the blocky effect. The applications of the proposed method can be extended to tackle image segmentation, image inpainting, image dehazing, image deblurring problems, and Rayleigh noise as well which occurs in ultrasound images.

In this work, we employ just the Canny edge detector and the local variance. For instance, when we approximate the textured region, we ignore some texture characteristics of pixels such as scales, direction, etc. In the next work, we require to enhance the structure detector methodology more to point out the structures adaptively in distinct routes and scales and then make the proposed algorithm perform better. Furthermore, the proposed method is still not a hundred percent effective for avoiding the staircase effect. To tackle this issue, we will improve the proposed method and algorithm to effectively and efficiently handle this problem.

We shall also proceed in the area of deep mathematical analysis of the model and proving the convergence of the techniques and optimizing the order of the equation used for the de-noising. Developing some fast schemes for solving differential equations derived from the minimization of the energy functional might be considered in future research.

We have used the adaptive method to select the best value of lambda for all the numerical simulations in this article which is sometimes quite hard to choose the best-selected value. This problem is under intense study and results will be reported in the subsequent paper.

REFERENCES

[1] N. Chumchob, K. Chen, and C. Brito-Loeza, "A new variational model for removal of combined additive and multiplicative noise and a fast algorithm for its numerical approximation," *Int. J. Comput. Math.*, vol. 90, no. 1, pp. 140–161, Jan. 2013.

[2] G. Aubert and P. Kornprobst, *Mathematical Problems in Image Processing of Applied Mathematical Sciences*, vol. 147. Berlin, Germany: Springer, 2000.

[3] F. Li, C. Shen, J. Fan, and C. Shen, "Image restoration combining a total variational filter and a fourth-order filter," *J. Vis. Commun. Image Represent.*, vol. 18, no. 4, pp. 322–330, Aug. 2007.

[4] Y. Xiao, T. Zeng, J. Yu, and M. K. Ng, "Restoration of images corrupted by mixed Gaussian-impulse noise via l_1–l_0 minimization," *Pattern Recognit.*, vol. 44, no. 8, pp. 1708–1720, Aug. 2011, doi: 10.1016/j.patcog.2011.02.002.

[5] F. Sciacchitano, Y. Dong, and T. Zeng, "Variational approach for restoring blurred images with Cauchy noise," *SIAM J. Imag. Sci.*, vol. 8, no. 3, pp. 1894–1922, Jan. 2015, doi: 10.1137/140997816.

[6] T. Le, R. Chartrand, and T. J. Asaki, "A variational approach to reconstructing images corrupted by Poisson noise," *J. Math. Imag. Vis.*, vol. 27, no. 3, pp. 257–263, Apr. 2007, doi: 10.1007/s10851-007-0652-y.

[7] L. I. Rudin, S. Osher, and E. Fatemi, "Nonlinear total variation based noise removal algorithms," *Phys. D, Nonlinear Phenomena*, vol. 60, nos. 1–4, pp. 259–268, Nov. 1992.

[8] J. Zhang and Z. Wei, "Fractional variational model and algorithm for image denoising," in *Proc. 4th Int. Conf. Natural Comput.*, vol. 5, Oct. 2008, pp. 524–528, doi: 10.1109/ICNC.2008.172.

[9] Z. Jun and W. Zhihui, "A class of fractional-order multi-scale variational models and alternating projection algorithm for image denoising," *Appl. Math. Model.*, vol. 35, no. 5, pp. 2516–2528, May 2011.

[10] C. F. B. Loeza, "Fast numerical algorithms for high order PDEs with application to image restoration techniques," Univ. Liverpool, Liverpool, U.K., Tech. Rep. 0000 0004 2697 3652, 2009.

[11] M. A. Khan, W. Chen, A. Ullah, and Z. Fu, "A mesh-free algorithm for ROF model," *EURASIP J. Adv. Signal Process.*, vol. 2017, no. 1, pp. 1–6, Dec. 2017, doi: 10.1186/s13634-017-0488-6.

[12] L.-L. Huang, L. Xiao, and Z.-H. Wei, "Multiplicative noise removal via a novel variational model," *EURASIP J. Image Video Process.*, vol. 2010, pp. 1–16, Dec. 2010.

[13] A. Ullah, W. Chen, and M. A. Khan, "A new variational approach for restoring images with multiplicative noise," *Comput. Math. Appl.*, vol. 71, no. 10, pp. 2034–2050, May 2016.

[14] G. Aubert and J.-F. Aujol, "A variational approach to removing multiplicative noise," *SIAM J. Appl. Math.*, vol. 68, no. 4, pp. 925–946, Jan. 2008.

[15] Y. Wu and X. Feng, "Speckle noise reduction via nonconvex high total variation approach," *Math. Problems Eng.*, vol. 10, Feb. 2015, Art. no. 627417.

[16] J. M. Bioucas-Dias and M. A. T. Figueiredo, "Total variation restoration of speckled images using a split-Bregman algorithm," in *Proc. 16th IEEE Int. Conf. Image Process. (ICIP)*, Cairo, Egypt, Nov. 2009, pp. 3717–3720.

[17] K. Krissian, C.-F. Westin, R. Kikinis, and K. G. Vosburgh, "Oriented speckle reducing anisotropic diffusion," *IEEE Trans. Image Process.*, vol. 16, no. 5, pp. 1412–1424, May 2007.

[18] J. W. Goodman, "Some fundamental properties of speckle," *J. Opt. Soc. Amer.*, vol. 66, no. 11, pp. 1145–1150, Nov. 1976.

[19] G. Liu, X. Zeng, F. Tian, Z. Li, and K. Chaibou, "Speckle reduction by adaptive window anisotropic diffusion," *Signal Process.*, vol. 89, no. 11, pp. 233–243, 2009, doi: 10.1016/j.sigpro.2009.04.042.

[20] M. A. Khan, A. B. Altamimi, Z. H. Khan, K. S. Khattak, S. Khan, A. Ullah, and M. Ali, "Multiquadric radial basis function approximation scheme for solution of total variation based multiplicative noise removal model," *Comput. Model. Eng. Sci.*, vol. 126, no. 1, pp. 55–88, 2021, doi: 10.32604/cmes.2021.011163.

[21] X.-G. Lv, J. Le, J. Huang, and L. Jun, "A fast high-order total variation minimization method for multiplicative noise removal," *Math. Problems Eng.*, vol. 2013, pp. 1–13, Jan. 2013.

[22] Y. Hao and J. Xu, "An effective dual method for multiplicative noise removal," *J. Vis. Commun. Image Represent.*, vol. 25, no. 2, pp. 306–312, Feb. 2014.

[23] B. Shi, L. Huang, and Z. Pang, "Fast algorithm for multiplicative noise removal," *J. Vis. Commun. Image R.*, vol. 23, no. 1, pp. 126–133, 2012.

[24] J. Shi and S. Osher, "A nonlinear inverse scale space method for a convex multiplicative noise model," *SIAM J. Imag. Sci.*, vol. 1, no. 3, pp. 294–321, Jan. 2008.

[25] X. Hu and Y. Hu, "A variational model for removing multiple multiplicative noises," *Open J. Appl. Sci.*, vol. 5, no. 12, pp. 783–796, 2015.

[26] H. Sun, Y. Zhang, D. Baleanu, W. Chen, and Y. Chen, "A new collection of real world applications of fractional calculus in science and engineering," *Commun. Nonlinear Sci. Numer. Simul.*, vol. 64, pp. 213–231, Nov. 2018, doi: 10.1016/j.cnsns.2018.04.019.

[27] G.-C. Wu, "A fractional variational iteration method for solving fractional nonlinear differential equations," *Comput. Math. Appl.*, vol. 61, no. 8, pp. 2186–2190, Apr. 2011, doi: 10.1016/j.camwa.2010.09.010.

[28] D. Chen, S. Sun, C. Zhang, Y. Chen, and D. Xue, "Fractional-order TV-L^2 model for image denoising," *Central Eur. J. Phys.*, vol. 41, no. 15, pp. 1–13, 2013.

[29] Y.-L. You and M. Kaveh, "Fourth-order partial differential equations for noise removal," *IEEE Trans. Image Process.*, vol. 9, no. 10, pp. 1723–1730, Oct. 2000.

[30] M. R. Hajiaboli, "A self-governing fourth-order nonlinear diffusion filter for image noise removal," *IPSJ Trans. Comput. Vis. Appl.*, vol. 2, no. 3, pp. 94–103, Mar. 2010.

[31] M. A. Khan, W. Chen, A. Ullah, and L. Ji, "Euler's elastica and curvature based model for image restoration," *PLoS ONE*, vol. 13, no. 9, Sep. 2018, Art. no. e0202464, doi: 10.1371/journal.pone.0202464.

[32] D. Chen, Y. Chen, and D. Xue, "Three fractional-order TV-L^2 models for image denoising," *J. Comput. Inf. Syst.*, vol. 9, no. 12, pp. 4773–4780, 2013.

[33] D. Chen, Y. Chen, and D. Xue, "Fractional-order total variation image restoration based on primal-dual algorithm," *Abstract Appl. Anal.*, vol. 2013, Nov. 2013, Art. no. 585310.

[34] Y.-F. Pu, J.-L. Zhou, and X. Yuan, "Fractional differential mask: A fractional differential-based approach for multiscale texture enhancement," *IEEE Trans. Image Process.*, vol. 19, no. 2, pp. 491–511, Feb. 2010.

[35] J. Zhang, Z. Wei, and L. Xiao, "A fast adaptive reweighted residual-feedback iterative algorithm for fractional-order total variation regularized multiplicative noise removal of partly-textured images," *Signal Process.*, vol. 98, pp. 381–395, May 2014.

[36] V. B. S. Prasath, N. H. T. Dang, Q. H. Nguyen, and M. H. Le, "Multiscale gradient maps augmented Fisher information-based image edge detection," *IEEE Access*, vol. 8, pp. 141104–141110, 2020.

[37] J. Shi, H. Jin, and Z. Xiao, "A novel hybrid edge detection method for polarimetric SAR images," *IEEE Access*, vol. 8, pp. 8974–8991, 2020.

[38] J. Zhang and K. Chen, "A total fractional-order variation model for image restoration with nonhomogeneous boundary conditions and its numerical solution," *SIAM J. Imag. Sci.*, vol. 8, no. 4, pp. 2487–2518, Jan. 2015.

[39] Y. Pu, W. Wang, J. Zhou, Y. Wang, and H. Jia, "Fractional differential approach to detecting textural features of digital image and its fractional differential filter implementation," *Sci. China Ser. F, Inf. Sci.*, vol. 51, no. 9, pp. 1319–1339, Sep. 2008.

[40] P. Yi-Fei, "Fractional differential analysis for texture of digital image," *J. Algorithms Comput. Technol.*, vol. 1, no. 3, pp. 357–380, Oct. 2007.

[41] W. Feng, H. Lei, and Y. Gao, "Speckle reduction via higher order total variation approach," *IEEE Trans. Image Process.*, vol. 23, no. 4, pp. 1831–1843, Apr. 2014.

[42] Y.-M. Huang, M. K. Ng, and Y.-W. Wen, "A new total variation method for multiplicative noise removal," *SIAM J. Imag. Sci.*, vol. 2, no. 1, pp. 20–40, Jan. 2009.

[43] G. Steidl and T. Teuber, "Removing multiplicative noise by Douglas-Rachford splitting methods," *J. Math. Imag. Vis.*, vol. 36, no. 2, pp. 168–184, Feb. 2010.

[44] D. N. H. Thanh and S. D. Dvoenko, "A method of total variation to remove the mixed Poisson-Gaussian noise," *Pattern Recognit. Image Anal.*, vol. 26, no. 2, pp. 285–293, Apr. 2016.

[45] C. Li, Z. Ren, and L. Tang, "Multiplicative noise removal via using nonconvex regularizers based on total variation and wavelet frame," *J. Comput. Appl. Math.*, vol. 370, May 2020, Art. no. 112684, doi: 10.1016/j.cam.2019.112684.

[46] D. N. H. Thanh, V. B. S. Prasath, L. M. Hieu, and S. Dvoenko, "An adaptive method for image restoration based on high-order total variation and inverse gradient," *Signal, Image Video Process.*, vol. 14, no. 6, pp. 1189–1197, Sep. 2020.

MUSHTAQ AHMAD KHAN received the Ph.D. degree from the School of Engineering Mechanics and Materials, Hohai University, China. He is currently teaching with the Department of Electrical Engineering, University of Engineering and Technology, Mardan, Pakistan. His research interests include mathematical modeling and numerical simulation, mesh-based and meshless schemes in variational PDEs, filter-based image restoration models, algorithm analysial-order PDEs, fast numerical methods for the solution of integral order, and fractional order PDEs etc.

ASMAT ULLAH received the Ph.D. degree in engineering mechanics from Hohai University, Nanjing, China. He is currently working as a Subject Specialist/Lecturer in mathematics with the Department of Education, University of Engineering and Technology Peshawar, Peshawar, Pakistan. His research interests include image denoising, image segmentation, image de-hazing, fractional-order PDEs, fast numerical methods for the solution of integral order, and fractional order PDEs etc.

SAHIB KHAN received the Ph.D. degree in electrical electronics and communications engineering from the Politecnico di Torino, Italy. After his Ph.D. degree, he joined the University of Engineering and Technology Mardan, where he is still part of the institute. His area of research includes multimedia forensics and security, clustering, camera source identifications, steganography, and watermarking.

MURTAZA ALI received the Ph.D. degree in graph theory from the National University of Computer and Emerging Sciences, Peshawar, Pakistan. He is currently an Assistant Professor with the University of Engineering and Technology, Mardan, Pakistan. His research interests are in applied graph theory, combinatorics, algorithm analysial-order PDEs, fast numerical methods for the solution of integral order, and fractional order PDEs.

SHERAZ KHAN received the Ph.D. degree focus on the field of telecommunication engineering in wireless regional area networks (WRAN) from the Asian Institute of Technology (AIT), Thailand. He is currently an Assistant Professor with the University of Engineering Technology (UET) Mardan, Pakistan. His research interest includes resource allocation and delay analysis in WRANs, TV white spaces (TVWS), and smart grid communications. Further, he is actively engaged in the area of digital image restoration.

KHALIL KHAN received the B.S. degree in electrical engineering and the M.S. degree in computer engineering from the University of Engineering and Technology, Peshawar, Pakistan, in 2007 and 2012, respectively, and the Ph.D. degree from the Signals and Communication Laboratory, University of Brescia, Italy, in 2016. He is currently working as an Assistant Professor with the Department of Information Technology and Computer Science, Pak-Austria Fachhochschule: Institute of Applied Sciences and Technology, Pakistan. His research interests include a wide range of topics within digital image processing, machine learning, and computer vision.

MEHEDI MASUD (Senior Member, IEEE) received the Ph.D. degree in computer science from the University of Ottawa, Canada. He is a Professor with the Department of Computer Science, Taif University, Taif, Saudi Arabia. He has authored or coauthored around 70 publications, including refereed IEEE/ACM/Springer/Elsevier journals, conference papers, books, and book chapters. His research interests include machine learning, distributed algorithms, data security, formal methods, and health analytics. He has served as a technical program committee member in different international conferences. He was a recipient of many awards, including the Research in Excellence Award from Taif University. He is on the Associate Editorial Board of IEEE Access, *International Journal of Knowledge Society Research* (IJKSR), and Editorial Board Member of *Journal of Software*. He also served as a Guest Editor of *ComSIS Journal* and *Journal of Universal Computer Science* (JUCS). He is a member of ACM.

JEHAD ALI received the B.S. and M.S. degrees from the Department of Computer Systems Engineering, University of Engineering and Technology, Peshawar, Pakistan, in 2008 and 2016, respectively, the Ph.D. degree from the Department of Computer Engineering, Graduate School, Ajou University, South Korea, in February 2020. From 2011 to 2016, he worked as a Computer Engineer at Ghulam Ishaq Khan Institute (GIKI) of Engineering Sciences and Technology, Topi, Pakistan. He is working as a Research Professor with Ajou University, South Korea. His research interests include software-defined networking, tactical networks, cognitive radio communications, the Internet of Things, wireless sensor networks, image processing, and machine learning and applications of machine learning in software-defined networking. He is a member of the IEEE and International Association of Computer Science and Information Technology (IACSIT). He has participated and presented in IEEE and other prestigious conferences, such as MobiSys (ACM), IEEE ICNC, IEEE IEMCON indexed by Scopus, DBLP and Google Scholar. He has edited a special issue as a Lead Guest Editor in *Computers, Materials and Continua*. Moreover, he is in the Reviewer Board of *Applied Sciences* journal. He has been reviewing papers for *Wireless Personal Communication* journal (Springer Netherlands), IEEE Access, IEEE Sensors, *PLOS One*, *Sensors*, *Electronics*, *Sustainability*, *Applied Sciences*, *Computer Networks* (Elsevier), and IEEE Communication Letters.

• • •